UNIVERSITÀ DEGLI STUDI DI TRIESTE

Dipartimento di Ingegneria e Architettura

COMPLEMENTARY INVESTIGATION TECHNIQUES

FOR FUEL CELLS AND WATER ELECTROLYSERS

Prof. Marco Bogar

A.A. 2023-2024

OUTLINE

1. Scanning Electron Microscopy
2. Transmission Electron Microscopy
3. Infrared Imaging
4. X-Ray Absorption Spectroscopy*
5. X-Ray Diffraction and Small-Angle X-Ray Scattering*
6. Neutron-based characterization techniques*

* Topic not asked at the exam

BIBLIOGRAPHY

Reference	Paragraph/Pages
PEM fuel cells diagnostic tools, Haijiang Wang, Xiao-Zi Yuan, Hui Li, (2012), CRC Press	Ch. 14,15, 16

Insights	Paragraph/Pages
2011, Wiley, Jens Als-Nielsen, Des McMorrow, Elements of Modern X-ray Physics; ISBN: 978-0-470-97394-3	
PEM fuel cells diagnostic tools, Haijiang Wang, Xiao-Zi Yuan, Hui Li, (2012), CRC Press	Ch. 13, 12

INTRODUCTION

Jiao K. et al., Nature, 595, (2021), 361–369

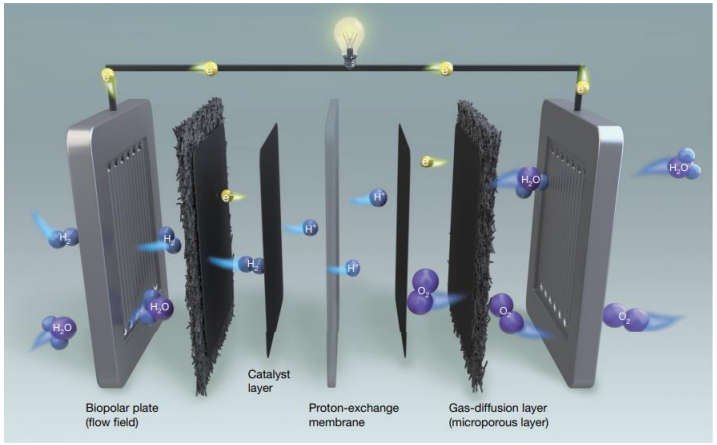

Electrode degradation

- High temperatures
- High humidity
- High potentials
- High gas crossover
- Gas starvation

Membrane degradation

- Mechanical degradation (stress and strain by alternating humidification temperatures)
- Chemical degradation (high temperatures and the presence of radicals)

- Is the fuel cell operating properly or are there any failures?
- Which degradation phenomena are taking place?
- How fast is degradation taking place?
- How the performances of a new material or component can be compared to the current standard?

CLASSIFICATION OF CHARACTERIZATION TECHNIQUES

Characterization techniques

Ex situ

Used to characterize some properties of individual components of the fuel cell once removed from the device in a non-operative form.

In situ

Used to characterize the performance of a single component of the cell in an environment with the same (or similar) characteristics found in a real device.

In operando

Used to characterize the performance of a single component or of a cell in real operative conditions.

Characterization techniques

Electrochemical

Based on recording of the electrical parameters

Micrographs

Based on recording of microscopic images (using different probes)

Optical

Radiation at different wavelengths is used to investigate specific sample properties

CLASSIFICATION OF CHARACTERIZATION TECHNIQUES

Characterization techniques

Ex situ

Used to characterize some properties of individual components of the fuel cell once removed from the device in a non-operative form.

In situ

Used to characterize the performance of a single component of the cell in an environment with the same (or similar) characteristics found in a real device.

In operando

Used to characterize the performance of a single component or of a cell in real operative conditions.

Characterization techniques

Electrochemical

Based on recording of the electrical parameters

Micrographs

Based on recording of microscopic images (using different probes)

Optical

Radiation at different wavelengths is used to investigate specific sample properties

EX SITU INVESTIGATION TECHNIQUES: ELECTRON MICROSCOPY

FROM BRIGHT FIELD MICROSCOPY TO ELECTRON MICROSCOPY

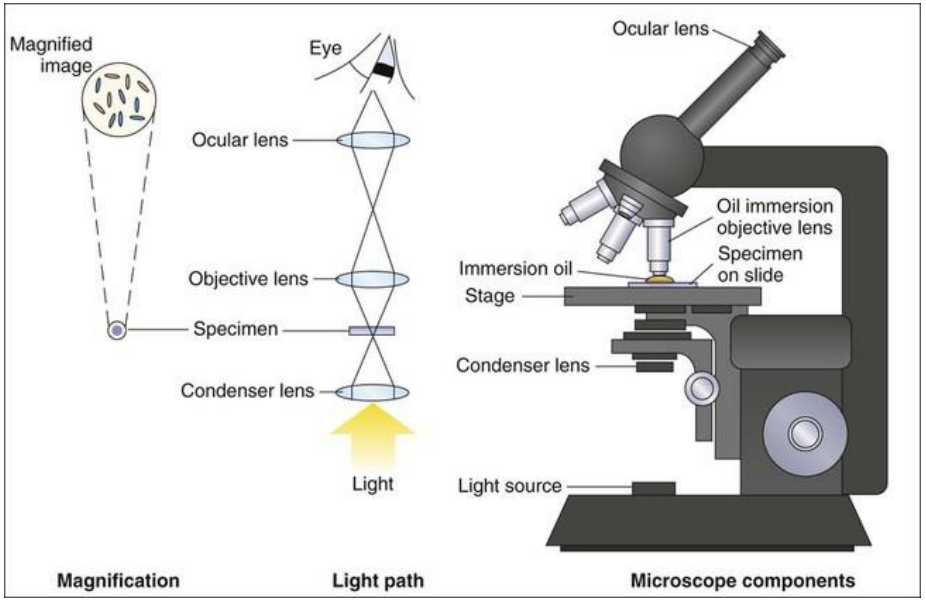

1995, William C Brown Pub. Ronald M. Atlas, Principles of Microbiology

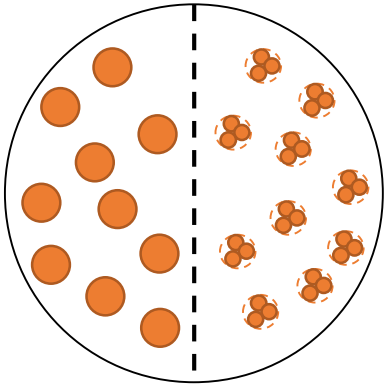

FROM BRIGHT FIELD MICROSCOPY TO ELECTRON MICROSCOPY

Starting from the discoveries of Ernst Abbe in 1873 about optics, the so called “The Abbe diffraction limit” could be formulated, stating that the smallest spot you can focus down to is related to the wavelength of used radiation as:

$$d = \frac{\lambda}{2\, n \sin\theta} \rightarrow d \propto \lambda \rightarrow d \geq \frac{\lambda}{2}$$

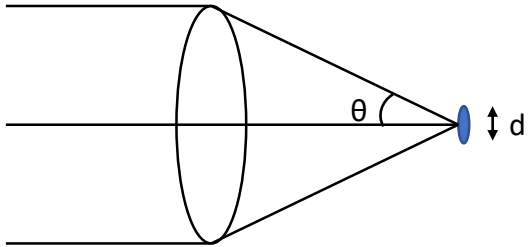

Light in the visible range of the spectra:

$$\lambda: 380 \div 750\ nm \rightarrow \lambda_{AV} = 565\ nm \rightarrow d_{min} \cong 280\ nm$$

FROM BRIGHT FIELD MICROSCOPY TO ELECTRON MICROSCOPY

According to wave/particle duality every particle can be considered either a particle or a wave.

In 1925 Louis de Broglie assumed that for particles are valid the same relations which were used for the photon, thus defining:

$$E = h\nu \qquad \lambda = c/\nu \qquad E = \frac{hc}{\nu} = pc$$

$$\lambda_B = \frac{h}{p} \quad \rightarrow \quad \lambda_B \propto \frac{1}{E}$$

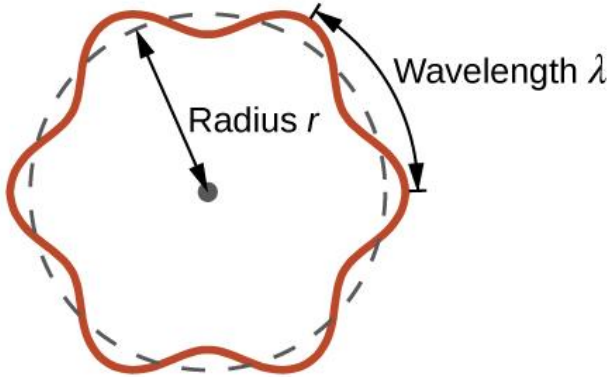

ELECTRON MICROSCOPY

Scanning Electron Microscope (SEM)

Resolution: from the micron-scale to some tens of nanometres

Costs: 150 000 to 1 000 000 $

Transmission Electron Microscope (TEM)

Resolution: nanometre

Costs: few 100 000 to 10 000 000 $

1. SCANNING ELECTRON MICROSCOPY

SCANNING ELECTRON MICROSCOPY (SEM)

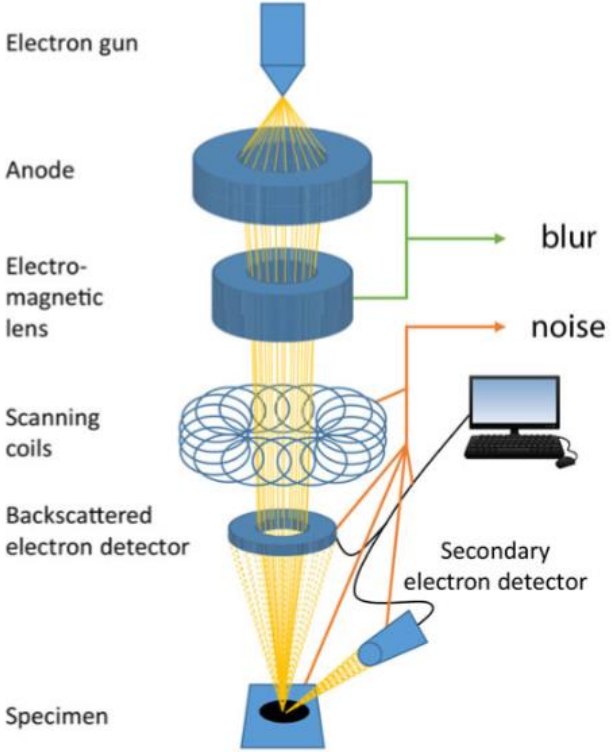

Roels J. et al., Journal of Microscopy, 271, 3, (2018), 239–254

After thermal-induced emission from an electron source (such as a tungsten wire or LaB_6), electrons are accelerated by an electrical field at first, to be further focused via electromagnetic lenses to a small spot on the specimen surface.

When hitting the sample surface, the primary electron beam penetrates into the specimen while scattering with its atoms. The interaction with the sample matter results in an energy loss of the primary electrons, related to the penetration depth within the so-called interaction volume (dependent on electron energy, usually around 1 µm).

SCANNING ELECTRON MICROSCOPY (SEM)

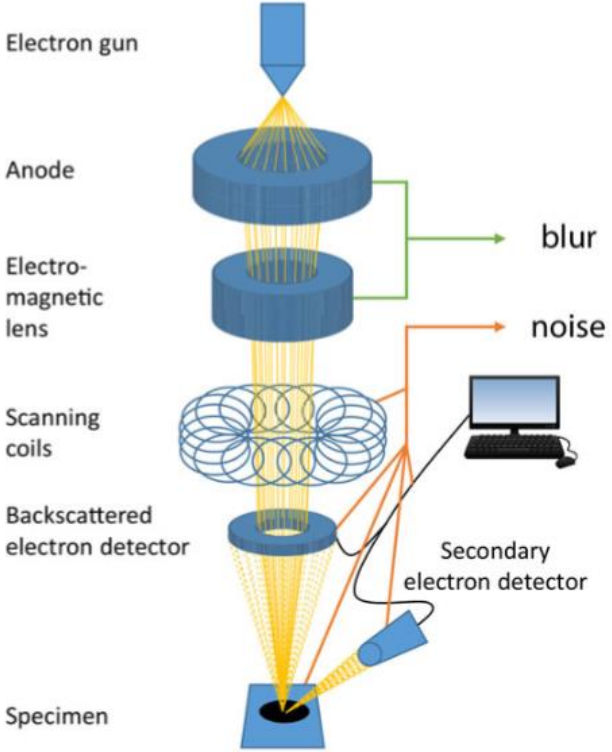

Roels J. et al., Journal of Microscopy, 271, 3, (2018), 239–254

When penetrating the sample surface the interaction among the impinging electrons and matter leads at the emission of two populations of electrons:

- Back-Scattered Electrons, via elastic scattering, thus with the same energy of the primary beam
- Secondary Electrons, via inelastic scattering, with lower energy with respect the primary beam

Electrons are then collected via two detectors which analyse electron energy and propagation direction.

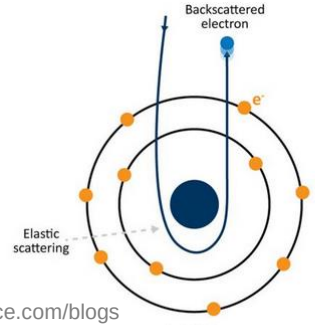

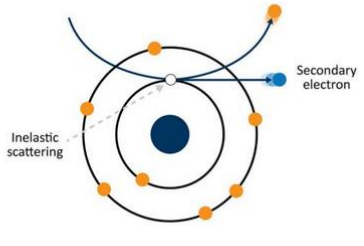

https://www.nanoscience.com/blogs/which-electron-detector-is-right-for-your-application/

SCANNING ELECTRON MICROSCOPY (SEM)

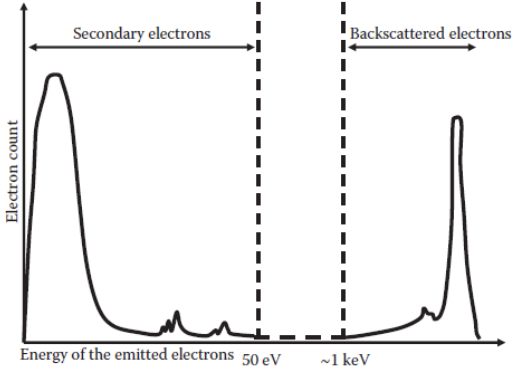

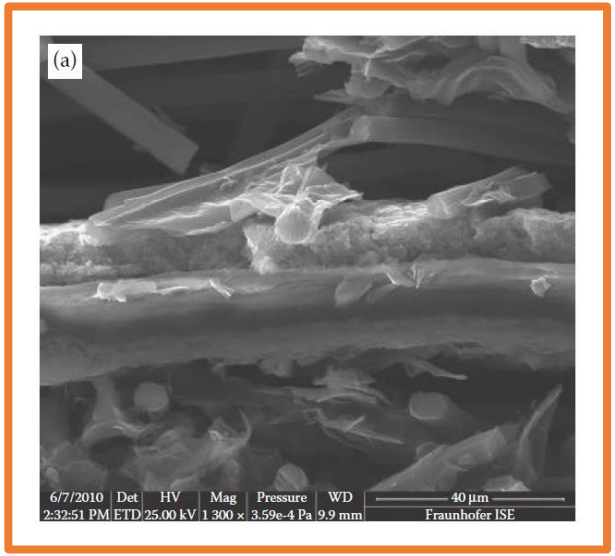

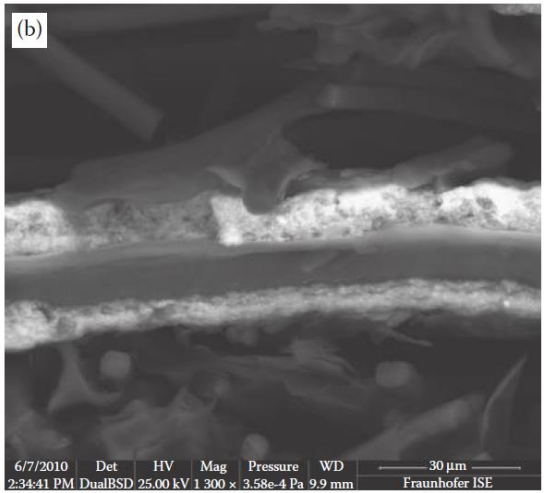

Elements with higher electron number scatter more than lighter ones, resulting in a stronger signal (i.e. cathode is more brighter because of the higher catalyst loading). Such dependence on the atomic number helps in distinguishing between different phases, conveying information on the sample composition.

SCANNING ELECTRON MICROSCOPY (SEM)

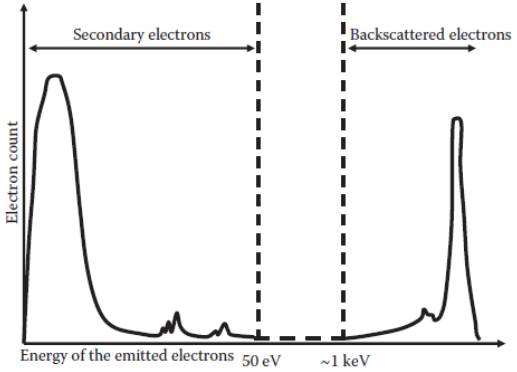

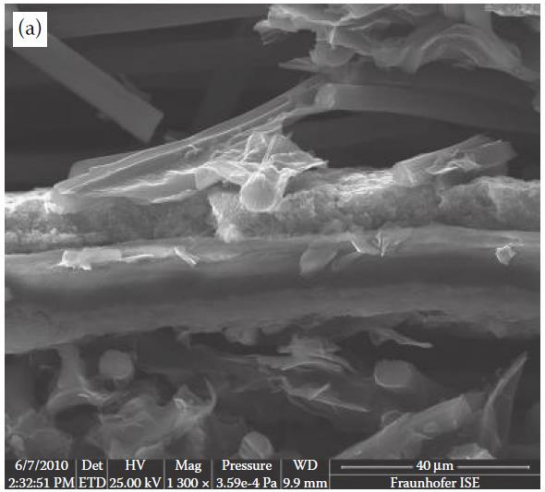

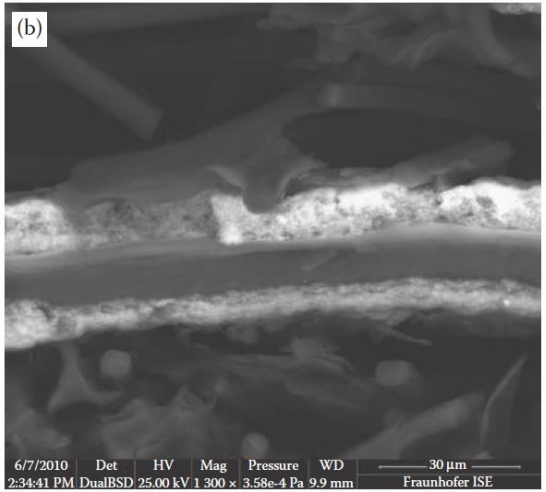

Secondary electrons are originated either from the surface or the near-surface regions. Containing lower energy than the backscattered electrons, they provide informatization about sample topography (that is, profile shape and surface roughness)

SCANNING ELECTRON MICROSCOPY (SEM)

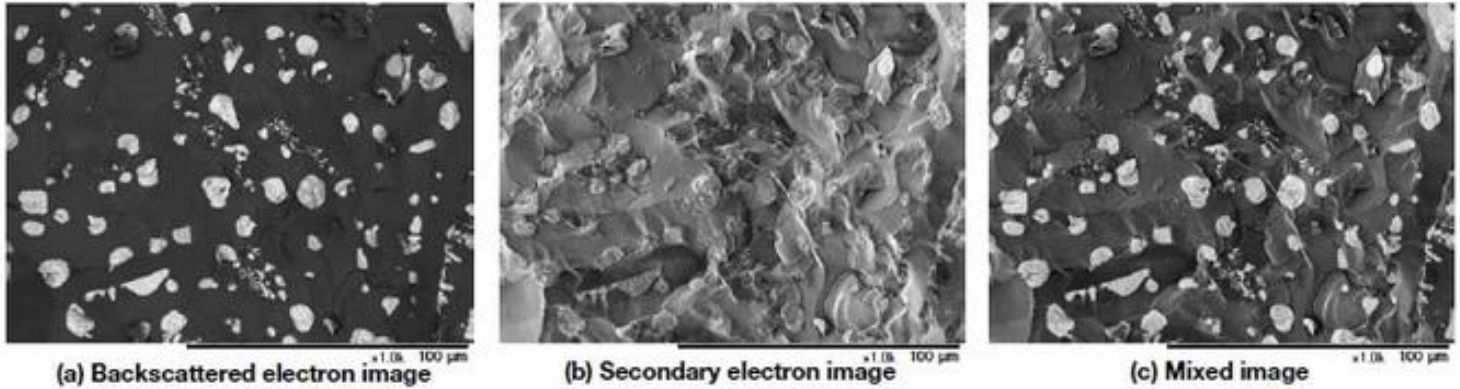

(a) Backscattered electron image (b) Secondary electron image (c) Mixed image

Fig.3 An example involving observations of a ruptured ceramic surface.
Accelerating voltage: Surface mode (5 kV)/ Observation mode: Standard mode (30 Pa)/ Magnification: 1,000×

SEM WITH ENERGY DISPERSIVE X-RAY SPECTROSCOPY (SEM-EDX)

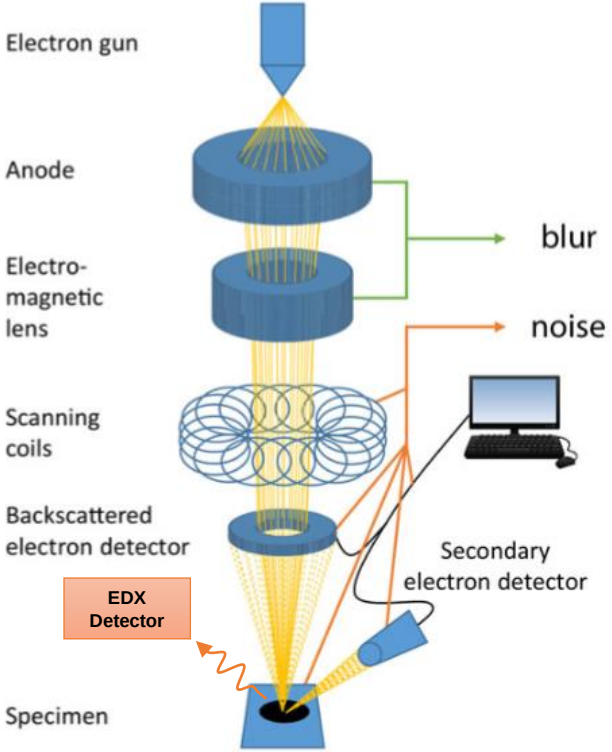

Roels J. et al., Journal of Microscopy, 271, 3, (2018), 239–254

Once a secondary electron is emitted from the atom, an electron from an outer shell can jump to fill the formed vacancy, releasing radiation (ranging from X-Rays to the visible spectra) which frequency is proportional to the energy gap between the two orbitals ($\Delta E = h\nu$). The energy difference between the inner and the outer shell is characteristic for the atomic structure of the element and thus the emitted photons carry information about the element from which they originate, and the chemical composition of the sample can be determined.

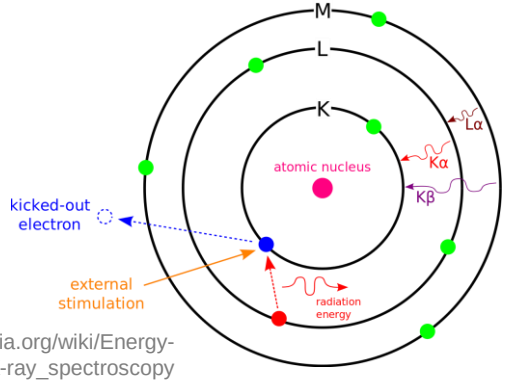

https://en.wikipedia.org/wiki/Energy-dispersive_X-ray_spectroscopy

SEM WITH ENERGY DISPERSIVE X-RAY SPECTROSCOPY (SEM-EDX)

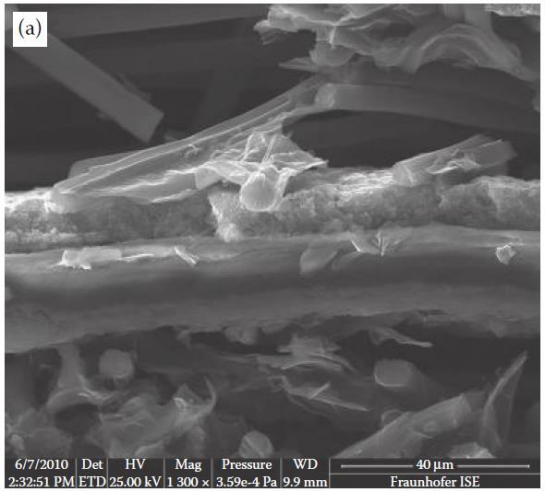

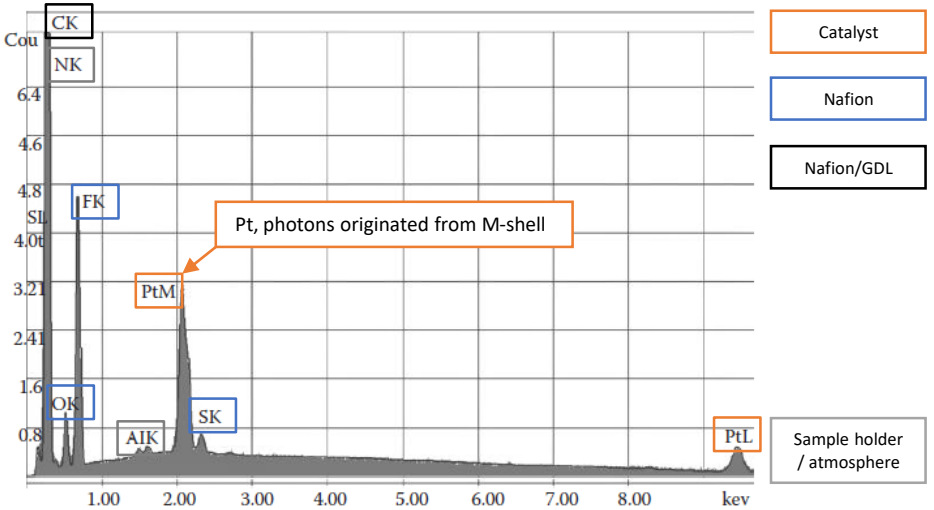

CROSS-SECTIONAL SEM – FOCUSED ION BEAM CUTTING

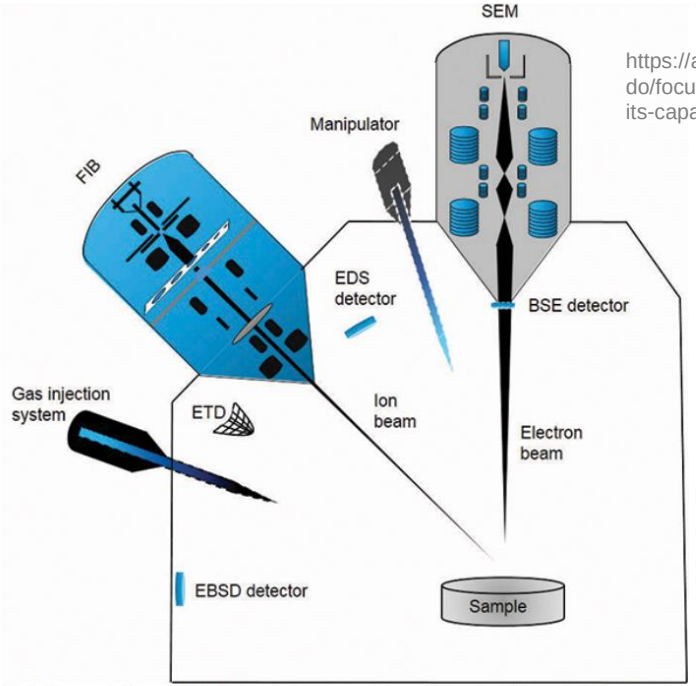

https://analyticalscience.wiley.com/content/article-do/focused-ion-beams-overview-technology-and-its-capabilities

Fig. 1: Commonly found FIB/SEM setup. FIB/ SEMs combine a SEM and a FIB in a single device and are often equipped with multiple detectors incl ETD, BSE, EDS, EBSD and in lens detectors. Gas injection systems as well as manipulators are commonly found on FIB/SEMs.

SEM – SOME EXAMPLES OF USE

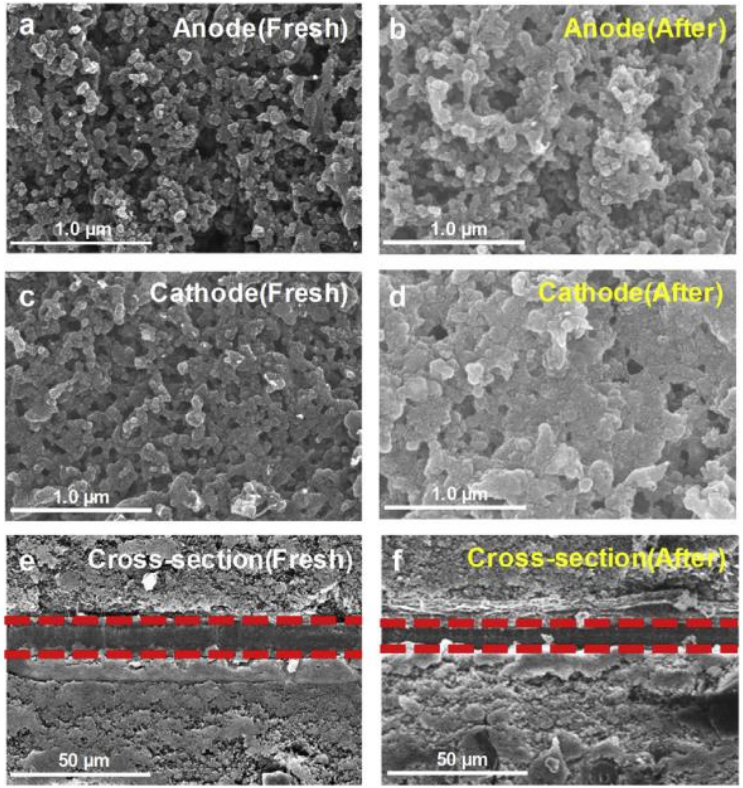

Microstructure and cross-sectional microstructure analyses before and after on-off cycling

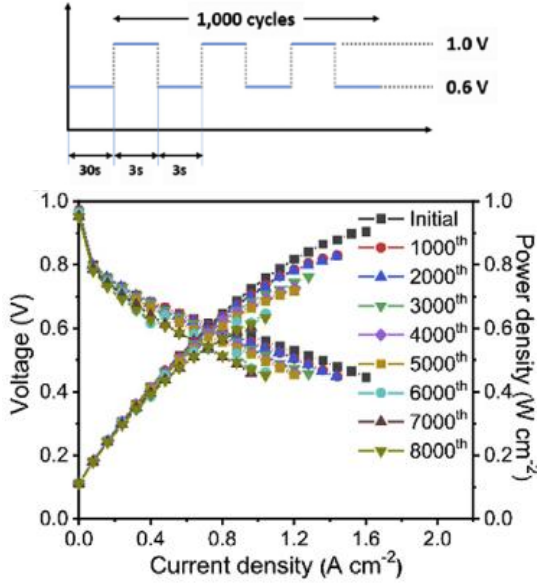

Choi S.R. et al., International Journal of Hydrogen Energy, 47, 39, (2022), 17379-17392

SEM – SOME EXAMPLES OF USE

Cross-sectional microstructure analyses before and after on-off cycling

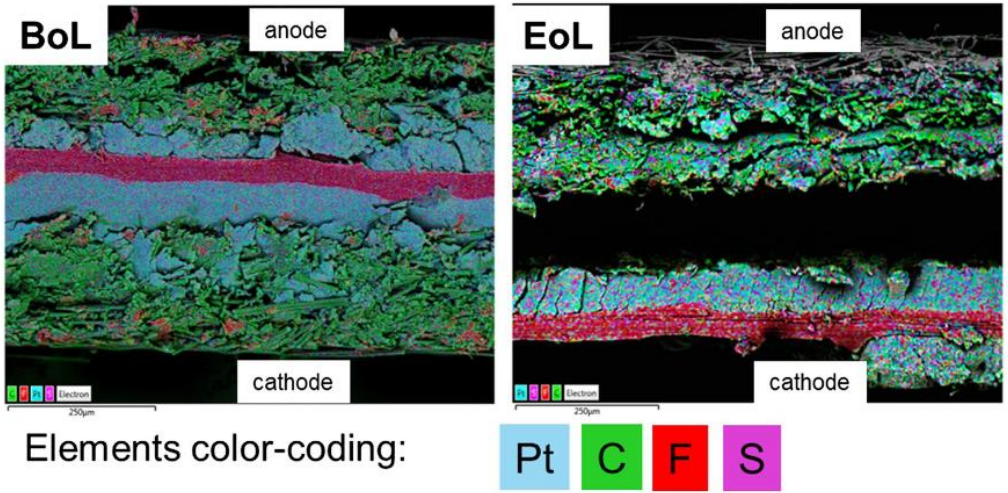

Table 1 Elemental composition of a pristine and tested MEA as obtained from HR-SEM/EDS

Test/element	BoL (wt%)	EoL (wt%)
Carbon	70.07	59.42
Fluoride	2.96	7.95
Sulphur	0.72	0.66
Platinum	26.26	27.21
Oxygen	–	4.76

Dyantyi N. et al., Materials for Renewable and Sustainable Energy, 8, 4, (2019)

SEM – SOME EXAMPLES OF USE

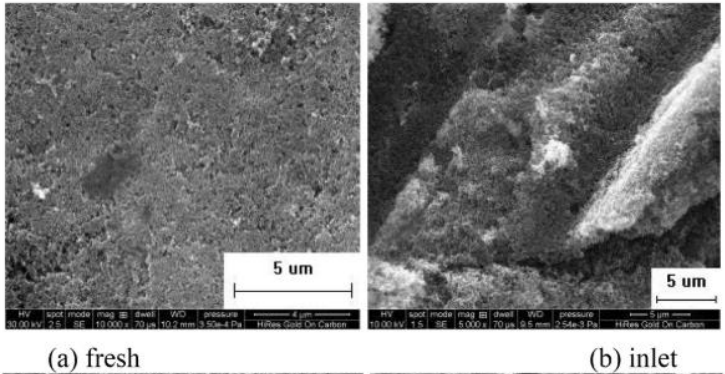

Fig. 10 – Scanning electron micrograph of the surface layer of cathode catalyst.

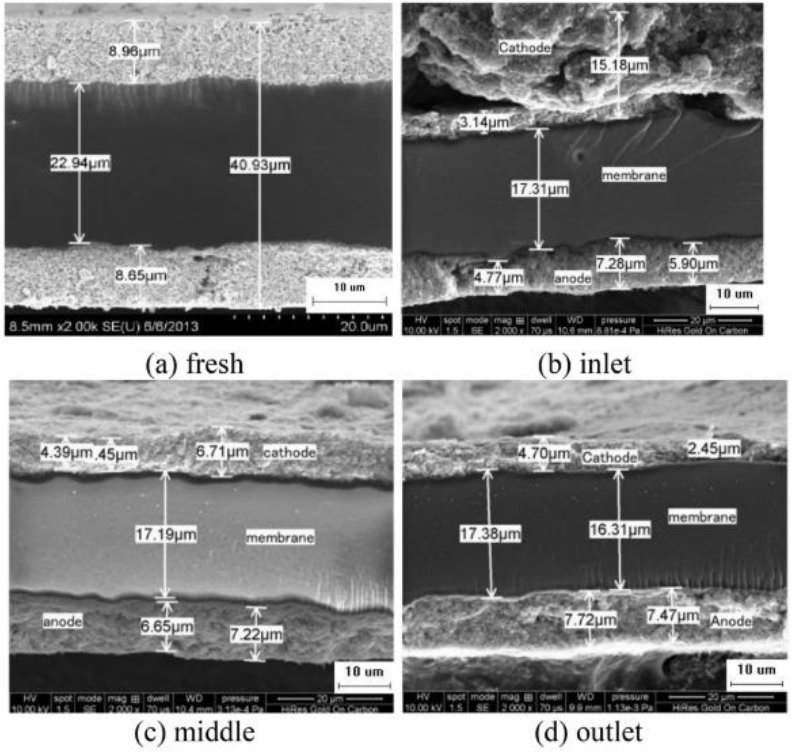

Fig. 11 – Cross-section of MEA morphology.

Shan J. et al., Int. J. Hydrogen Energy, 41, 7, (2016), 4239-4250

SEM – SOME EXAMPLES OF USE

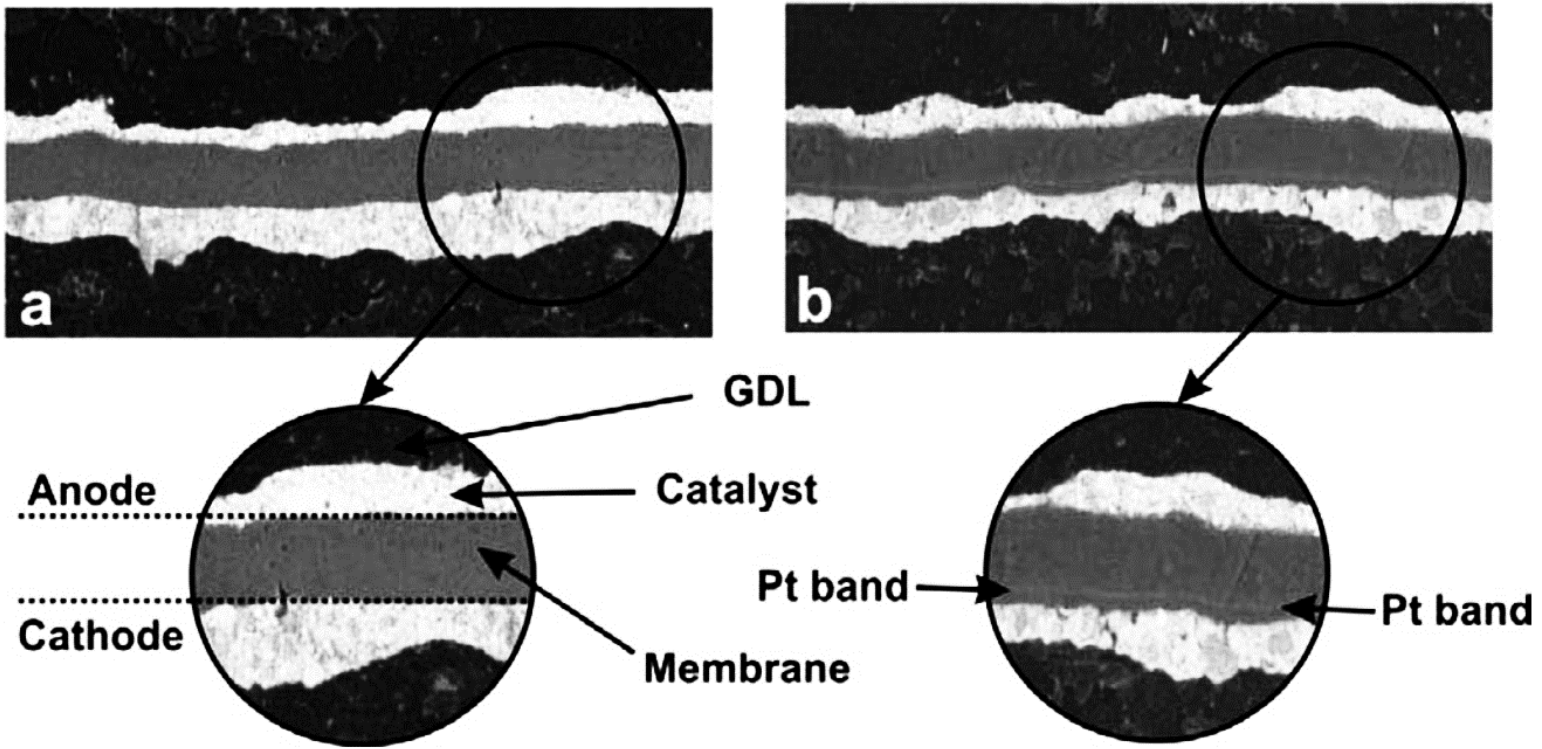

Macauley N. et al., ECS Electrochem. Lett. 2, (2013), F33

ENVIRONMENTAL SEM

In order to operate, SEM need to be enclosed in high vacuum (about 10^{-5} mbar), in order to increase the mean free path of the electrons. This fact introduces limitations about the type of samples that can be analyzed, which have to endure the vacuum. In addition, the vacuum system has to be tolerant to any degassing of the sample. Furthermore, sample surfaces need to be electrically connected to ground to avoid the charging of the sample, which would lead to local variations in electron emissions and deflecting of the primary electrons, resulting ultimately in artifacts. In this framework, in the last years, Environmental-SEM (ESEM) have been developed, allowing to keep the sample in a measurement chamber kept at atmospheric pressure, thus allowing to better analyze biological samples or samples in liquids. Moreover, such devices does not need biologic samples to be metal coated for being analyzed.

2. TRANSMISSION ELECTRON MICROSCOPY

TRANSMISSION ELECTRON MICROSCOPY (TEM)

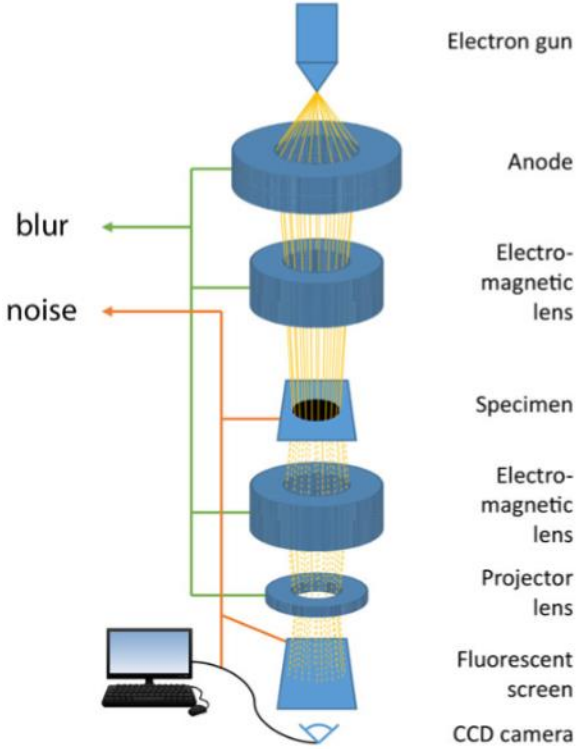

Roels J. et al., Journal of Microscopy, 271, 3, (2018), 239–254

In TEM (and in High Resolution TEM, HRTEM), the electron beam is accelerated by a potential ranging from 30 keV to 1MeV and addressed via a series of electromagnetic lenses on the sample. The transmitted electron beam is further directed onto a 2D detector producing a picture of the sample, with sub-nanometric resolution.

The high energy (and frequency) of the electrons allow to achieve atomic resolution, as long as sample thickness is thin enough to allow electron transmission.

Operating pressure is in the range of 10^{-4} Pa to 10^{-9} Pa, depending on the electron energy.

The impinging beam can be also focused to a size ranging from 0.05 – 0.2 nm and TEM can be carried out in scanning mode (STEM)

Also in TEM, EDX detector can be coupled for adding chemical sensitivity to the analysis.

TRANSMISSION ELECTRON MICROSCOPY (TEM)

TEM Grids Overview

The largest and most comprehensive selection of transmission electron microscopy grids, support films and SiN membranes for all TEM applications in life science, materials sciences, semiconductor and nanotechnology.

TEM Grids — Square & Hexagonal Mesh, Slot, Aperture & Index

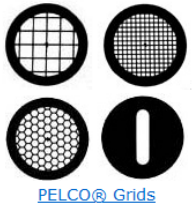

PELCO® Grids
Comprehensive selection of easy handling, wide rim, sturdy grids. Mesh, Hexagonal, Slot & Hole

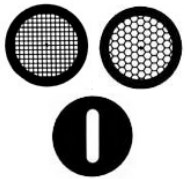

PELCO® Special Metal Grids
Stainless Steel, Titanium, Molybdenum, Aluminum

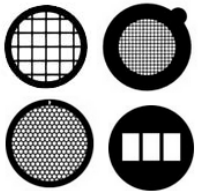

GILDER Grids
Large selection of well defined, thinner grids up to 2000 mesh. Mesh, Hexagonal, Slot & Hole

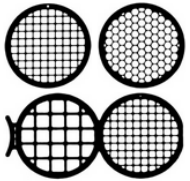

StrataTek™ Grids
Affordable, sturdy, medium mesh grids. Mesh, Hexagonal, Slot & Hole

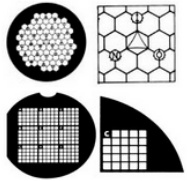

Reference / Finder Grids
Wide selection of reference, locator and micron index grids

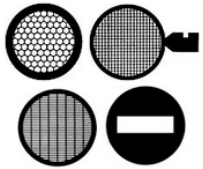

Veco Grids
Selection of rigid grids. Mesh, Hexagonal & Slot

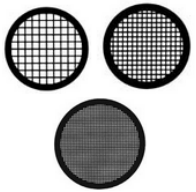

Maxtaform Grids
Selection of Rh coated grids

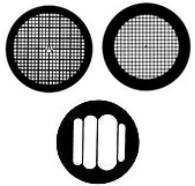

Athene Grids

https://www.tedpella.com/grids_html/grids.aspx

TEM FOR CATALYST CHARACTERIZATION – SOME EXAMPLES

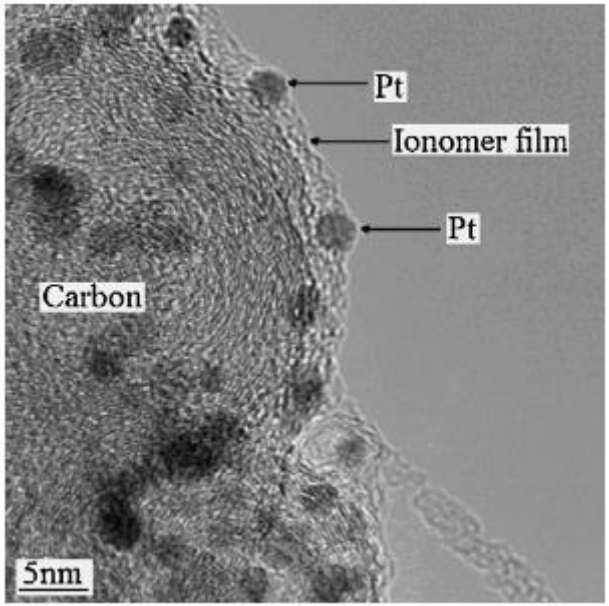

Holdcroft S., Chem. Mater. 2014, 26, 1, 381–393

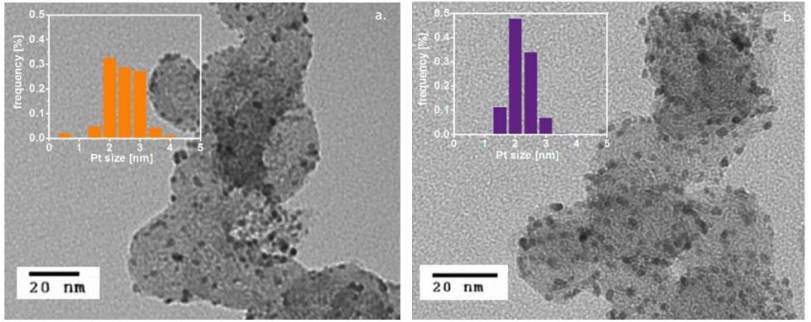

Orfanidi A. et al., Journal of The Electrochemical Society, 164, 4, (2017), F418-F426

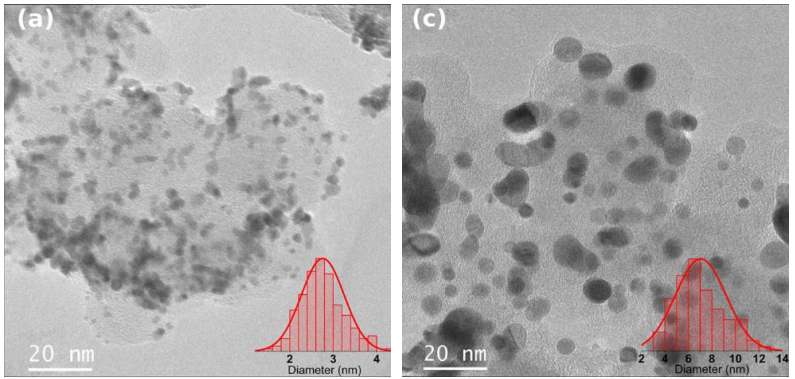

Bogar M. et al., International Journal of Hydrogen Energy 58 (2024) 1673–1681

TEM FOR CATALYST CHARACTERIZATION – SOME EXAMPLES

Dynamic growth of Pt_3Ni nanoparticles under atmospheric H_2/CO mixture gas

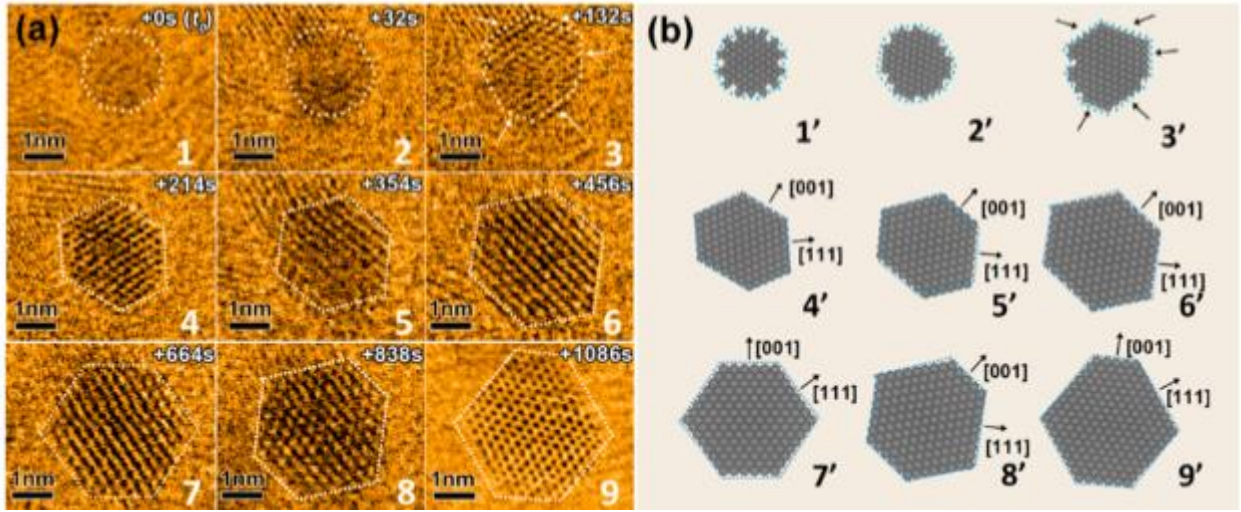

Chao H.S. et al, Chemical Reviews, 123, 13, (2023), 8041-8942

TEM FOR CATALYST CHARACTERIZATION – SOME EXAMPLES

Layer-by-layer growth of a (100) Pt shell on ordered Pt_3Co catalyst during oxygen annealing; (f–h) enlarged surface region.

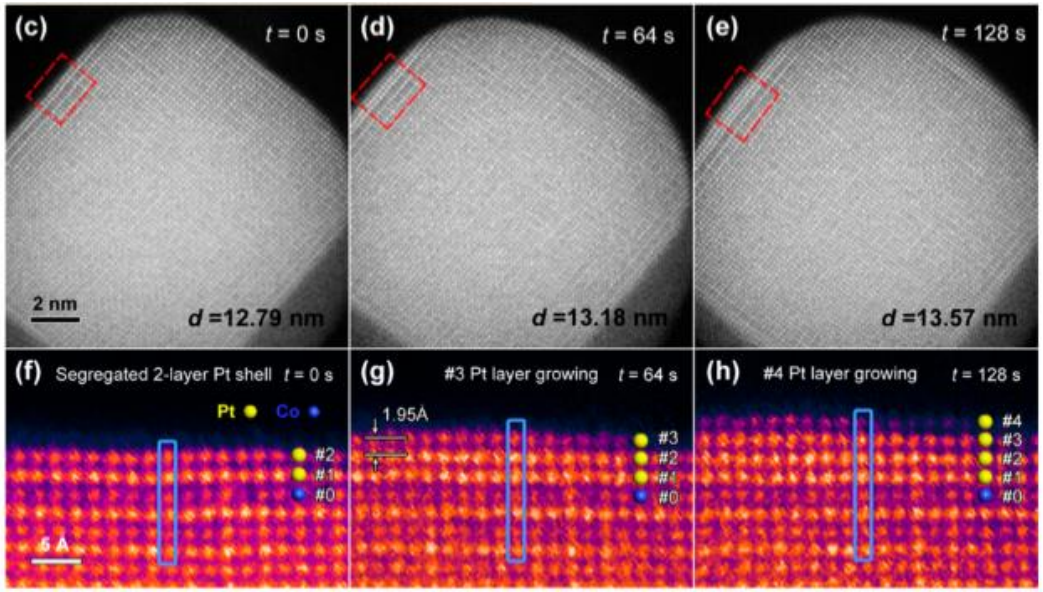

Chao H.S. et al, Chemical Reviews, 123, 13, (2023), 8041-8942

TEM FOR CATALYST CHARACTERIZATION – SOME EXAMPLES

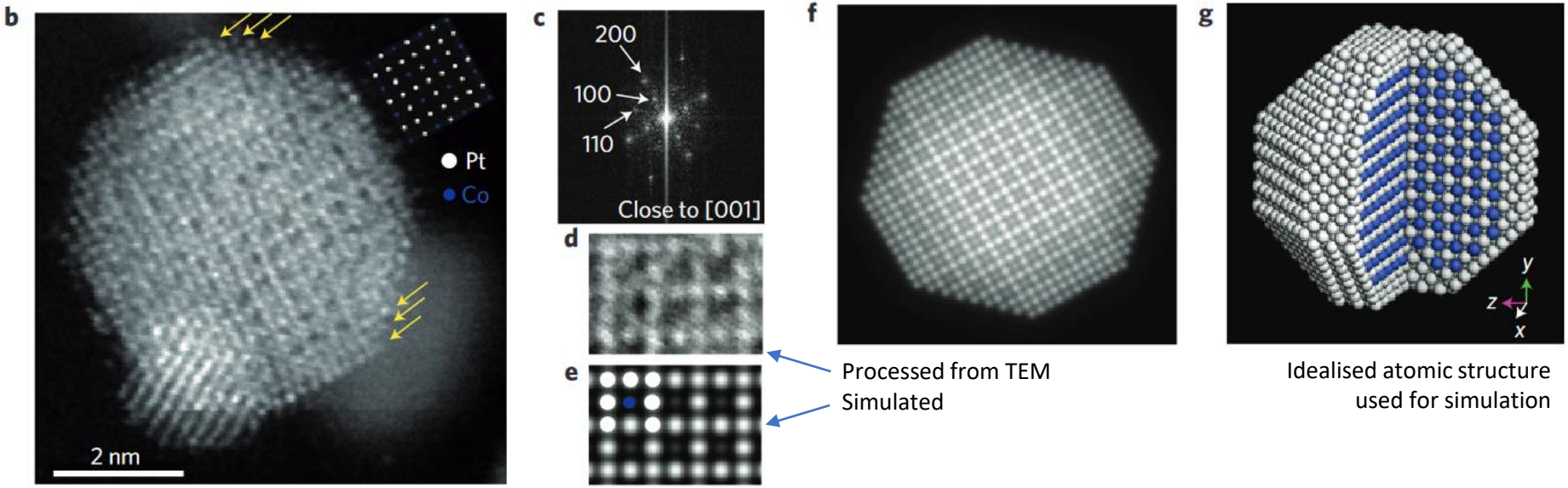

Processed from TEM
Simulated

Idealised atomic structure
used for simulation

Wang D. et al., Nature Materials, 12, (2013), 81–87

EELS OR EDX COUPLED TEM

EDX (or EDS) or Electron Energy Loss Spectroscopy (EELS) detectors can be coupled to TEM. While the former technique allows to obtain chemical-sensitive analysis, the latter one relies on the analysis of kinetic energy of electrons subject to inelastic scattering with the electrons bound with atoms composing the sample. In principle EELS allows to measure atomic composition, chemical bonding, valence and conduction band electronic properties, surface properties, and element-specific pair distance distrib

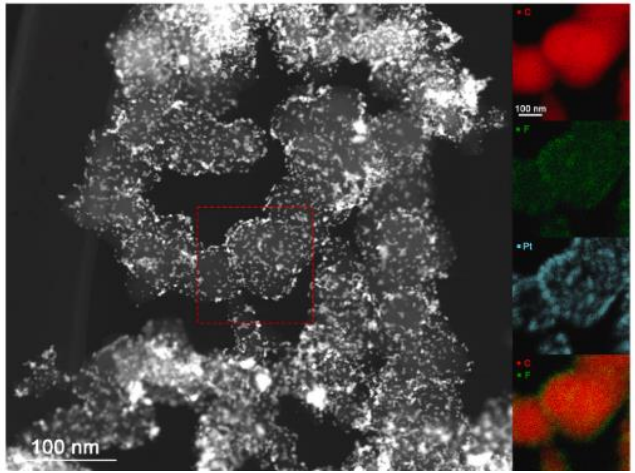

Yakovlev Y.V. et al., Journal of Power Sources 490 (2021) 229531

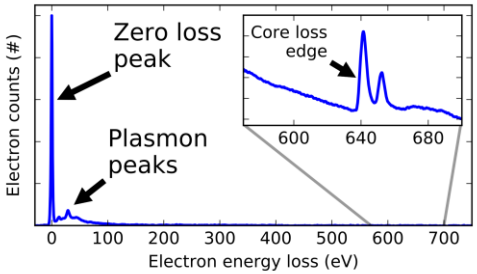

https://en.wikipedia.org/wiki/Electron_energy_loss_spectroscopy

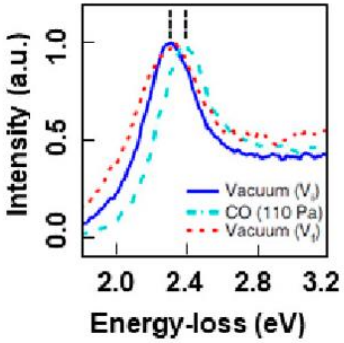

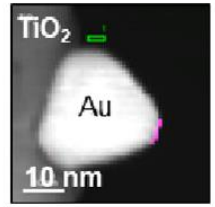

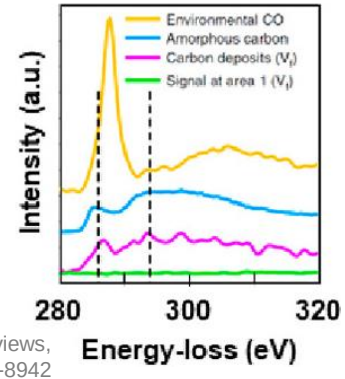

Chao H.S. et al, Chemical Reviews, 123, 13, (2023), 8041-8942

RADIATION-BASED INVESTIGATION TECHNIQUES

THE ELECTROMAGNETIC SPECTRUM

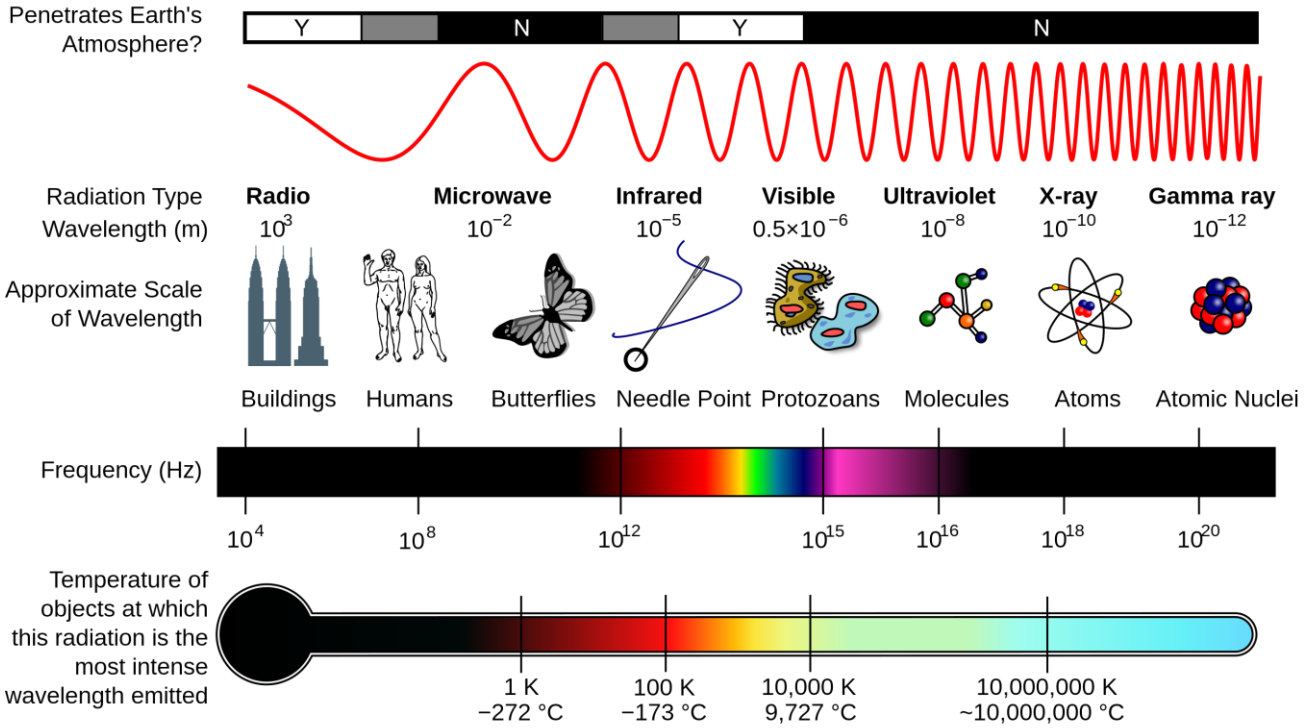

$$E = \frac{hc}{\lambda}$$

Sun Y., Materials Today, 15, 4, (2012), 140-147

3. INFRARED IMAGING

INFRARED IMAGING

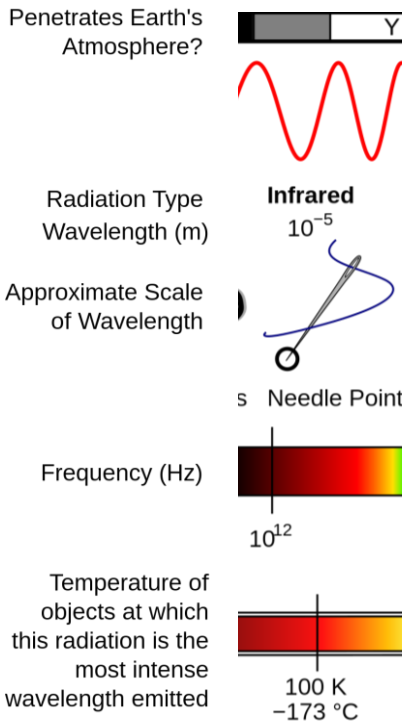

Sun Y., Materials Today, 15, 4, (2012), 140-147

Infrared (IR) imaging can be used to evaluate membrane thickness and hydrogen crossover in form of IR radiation generated from hydrogen and oxygen spontaneous recombination. It allows to perform fast, efficient, nonintrusive analyses (using open cathode cells), suitable for detecting defects, pinholes, or perforation, and adapt to quality control of continuous manufacturing.

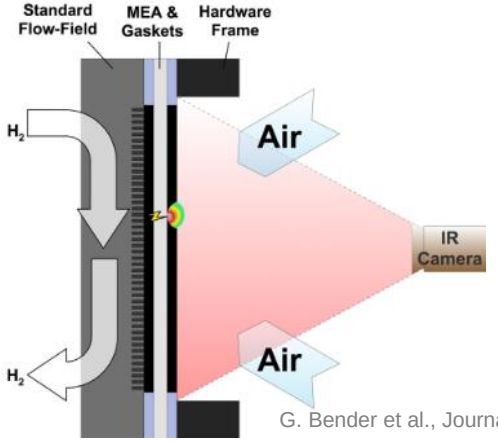

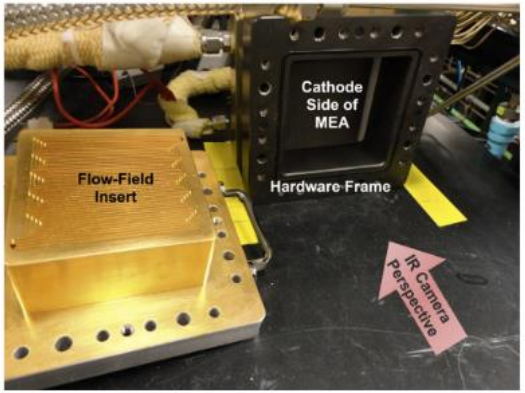

G. Bender et al., Journal of Power Sources, 253, (2014), 224-229

INFRARED IMAGING

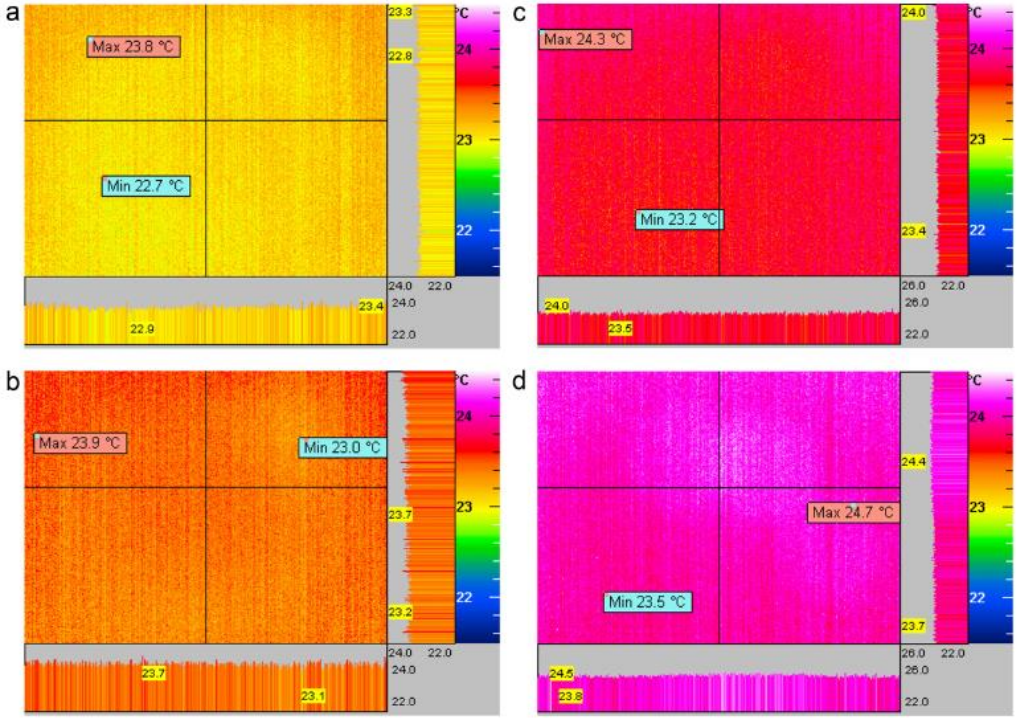

Fig. 7. Comparison of IR images for fresh MEA samples with different membranes using 5% H_2 in N_2: (a) fresh N117 MEA (average temp: 23.091 °C), (b) fresh N115 MEA (average temp: 23.429 °C), (c) fresh NR212 MEA (average temp: 23.724 °C), and (d) fresh NR211 MEA (average temp: 24.063 °C).

The thinner the membrane, the higher the average temperature and the greater the hydrogen crossover through the membrane, in agreement with LSV

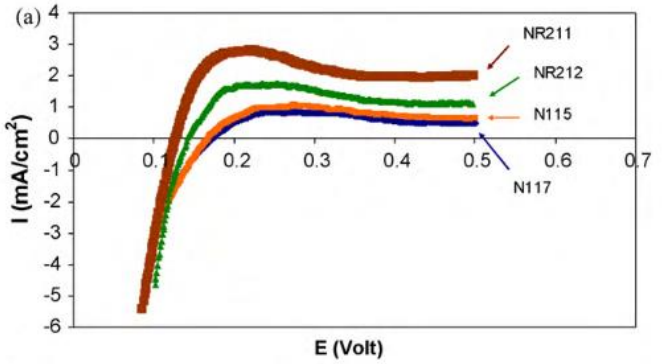

Yuan X.-Z. et al., Journal of Power Sources, 205, (2012), 324–334

Yuan X.-Z. et al., Journal of Power Sources, 195, (2010), 7594–7599

INFRARED IMAGING

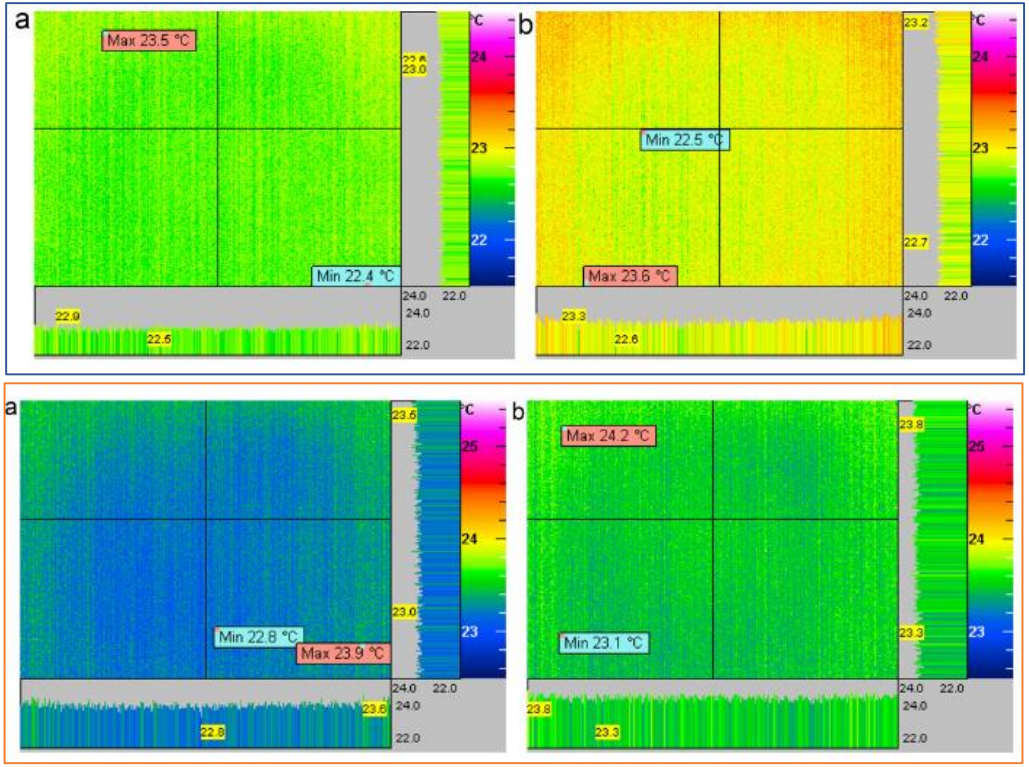

Thicker membranes showed lower increase of hydrogen crossover after 1000 h of degradation

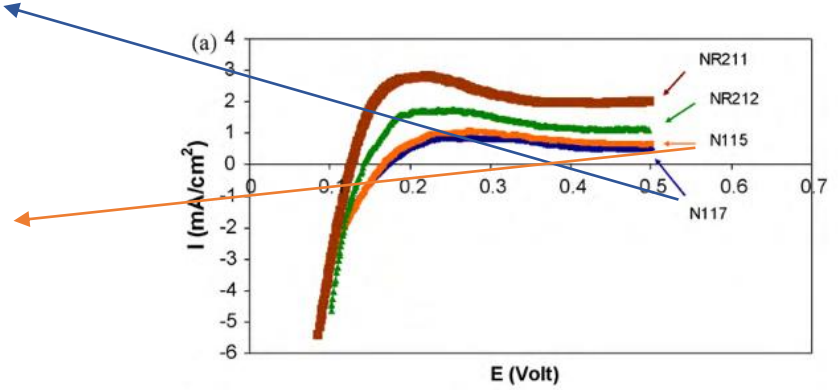

Yuan X.-Z. et al., Journal of Power Sources, 205, (2012), 324–334

Yuan X.-Z. et al., Journal of Power Sources, 195, (2010), 7594–7599

INFRARED IMAGING

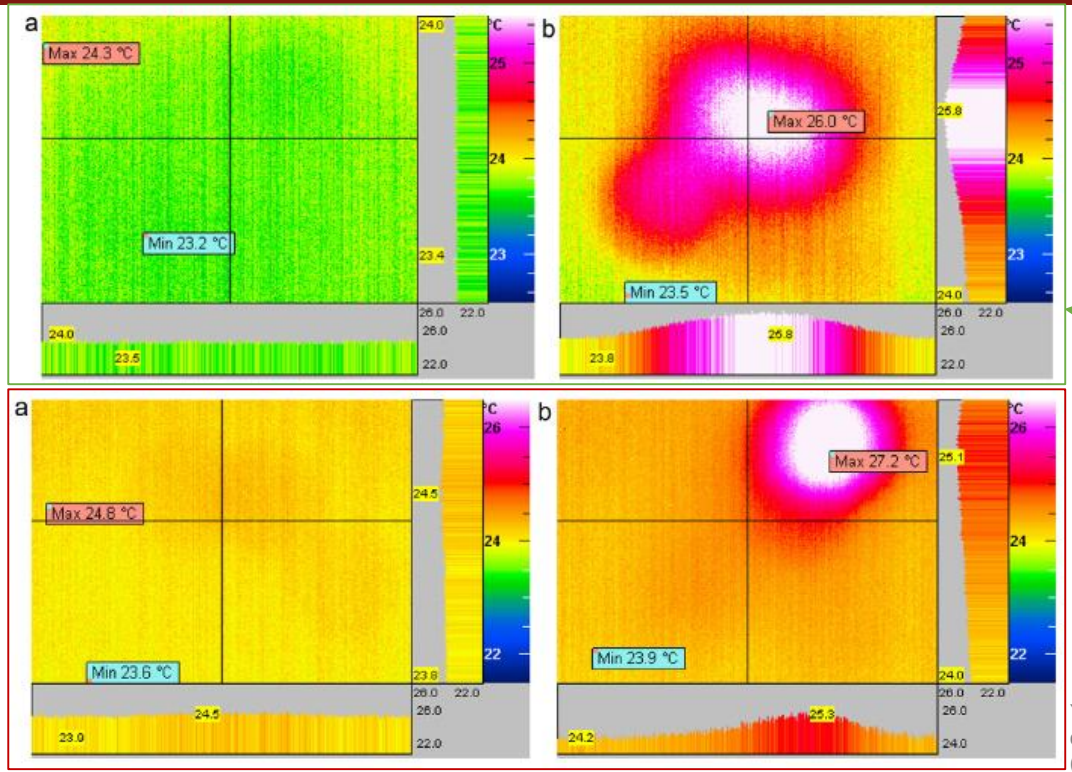

Thinner membranes show pinhole formation as well as a slight increase of background temperature, which made the author speculate that that for thinner membranes, pinholes are the major reason for membrane degradation, rather than membrane thinning.

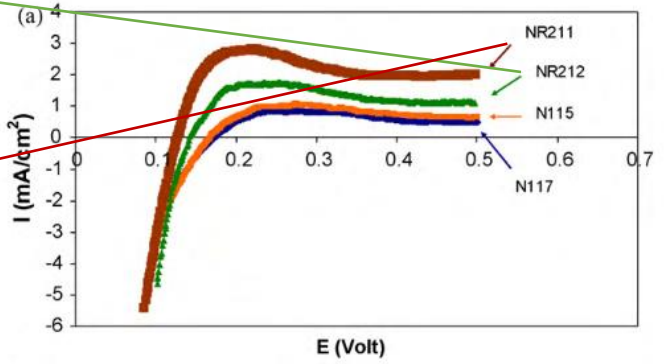

Yuan X.-Z. et al., Journal of Power Sources, 205, (2012), 324–334

Yuan X.-Z. et al., Journal of Power Sources, 195, (2010), 7594–7599

X-RAY BASED CHARACTERIZATION TECHNIQUES

X-RAY BASED CHARACTERIZATION TECHNIQUES

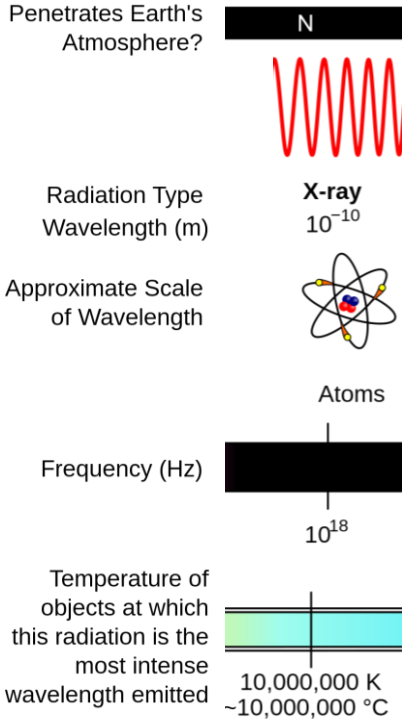

Sun Y., Materials Today, 15, 4, (2012), 140-147

X-Rays compose the electromagnetic radiation in the region of an Angstrom (10^{-10}m), more precisely they cover the range from 10^{-8} to 10^{-12} m.

They can be described in function of their wavelength or in function of their energy: usually at wavelengths bigger than 1 Å the Soft X-Ray region is defined, while at wavelengths of 1 Å or below, the Hard X-Ray can be found.

$$E = \frac{hc}{\lambda} \rightarrow E(keV) = \frac{12398}{\lambda(\text{Å})}$$

RADIATION – MATTER INTERACTION

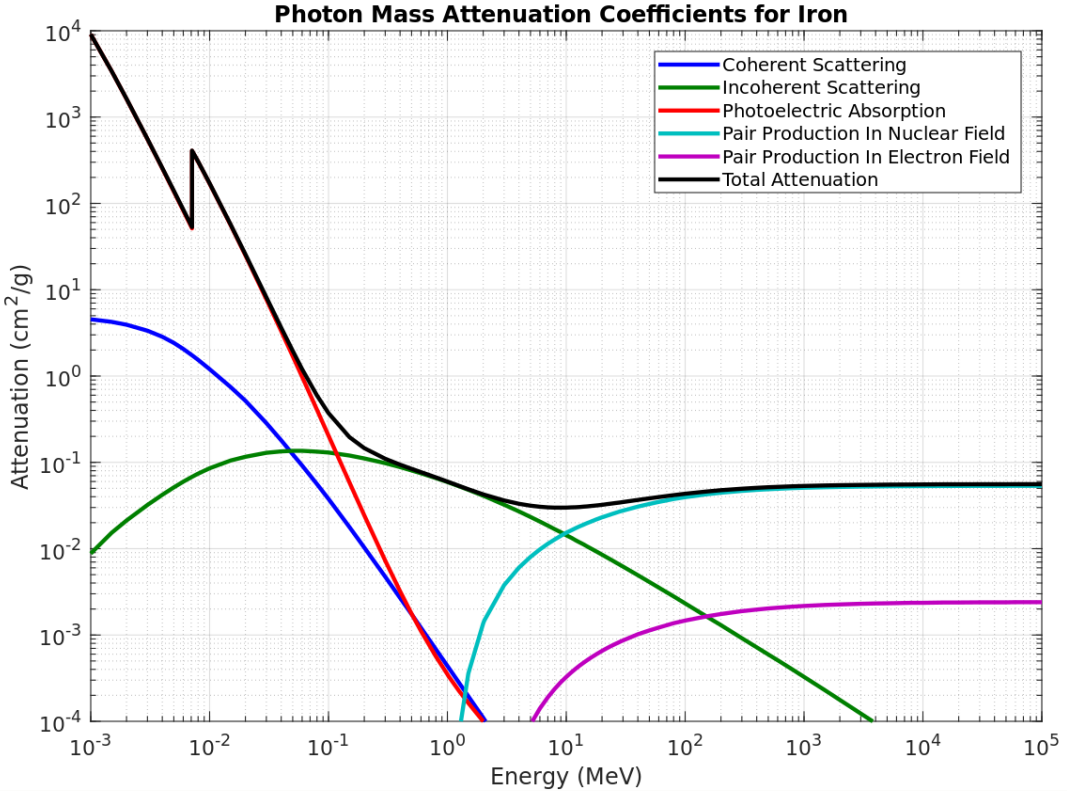

https://it.m.wikipedia.org/wiki/File:Ironattenuation.PNG

RADIATION – MATTER INTERACTION

(a) Photoelectric absorption

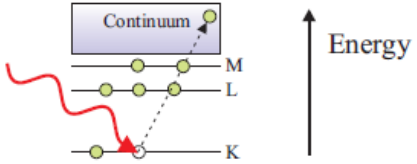

(b) Fluorescent X-ray emission

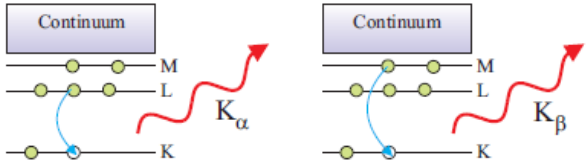

(c) Auger electron emission

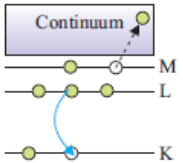

Nielsen, McMorrow, Elements of Modern X-ray Physics, Wiley (2011)

RADIATION – MATTER INTERACTION

X-Ray scattering

$\lambda \gg \overline{D} \rightarrow \lambda' = \lambda$ (Rayleigh)

$\lambda \sim \overline{D}$

$\lambda' > \lambda$ Inelastic (Compton)

$\lambda' = \lambda$ Elastic (Thomson)

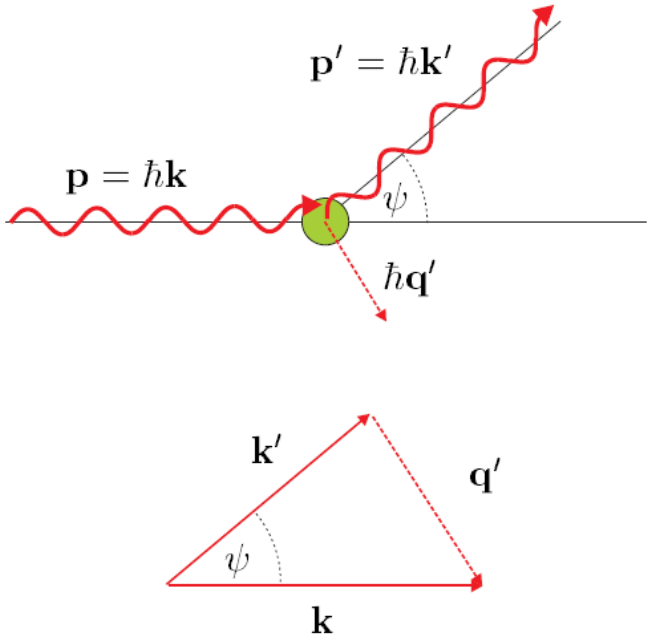

Nielsen, McMorrow, Elements of Modern X-ray Physics, Wiley (2011)

FACILITIES

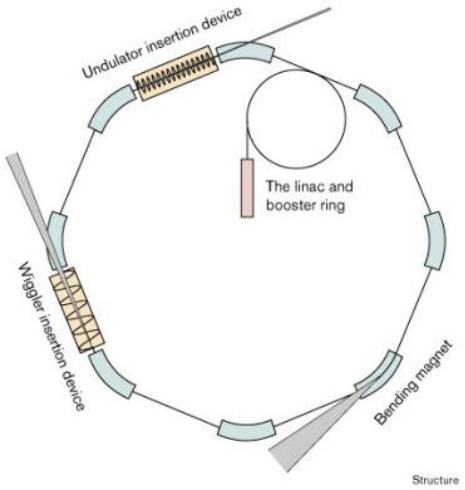

Mitchell E. et al., Structure 1999, Vol 7 No 5

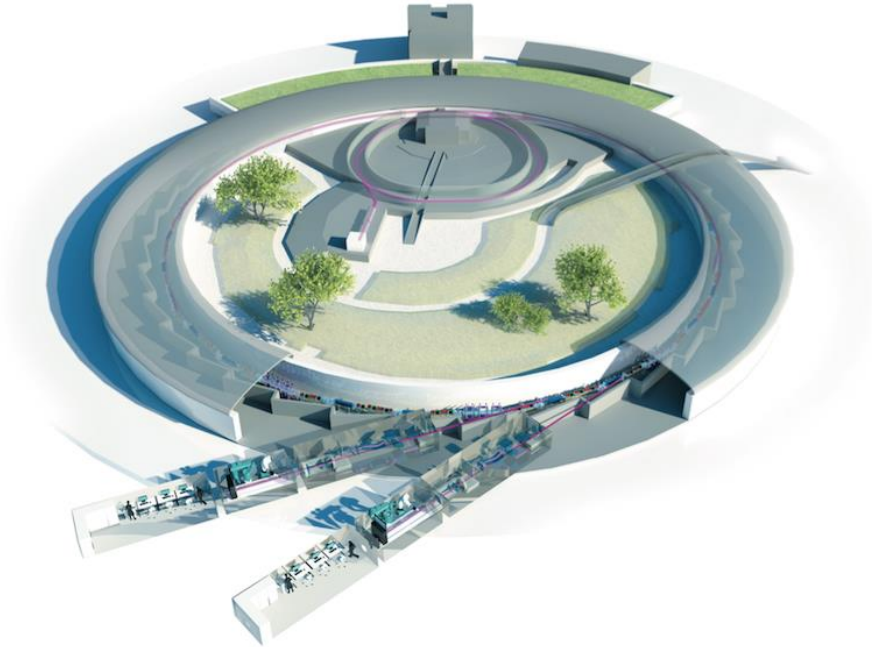

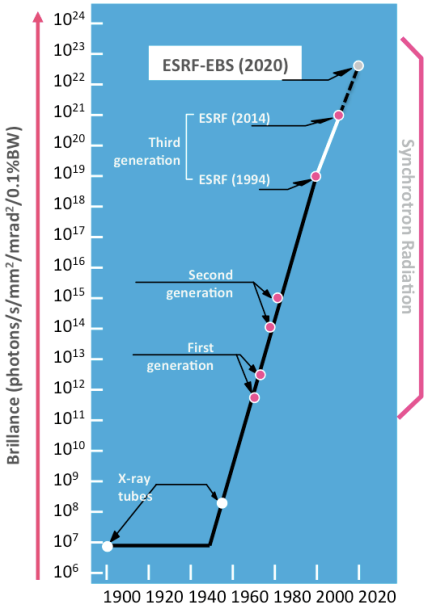

https://www.esrf.fr/home/UsersAndScience/Accelerators.html

EXPERIMENTAL POSSIBILITIES

Ex situ analysis
MEA are compared in pristine conditions and after having been aged/degraded

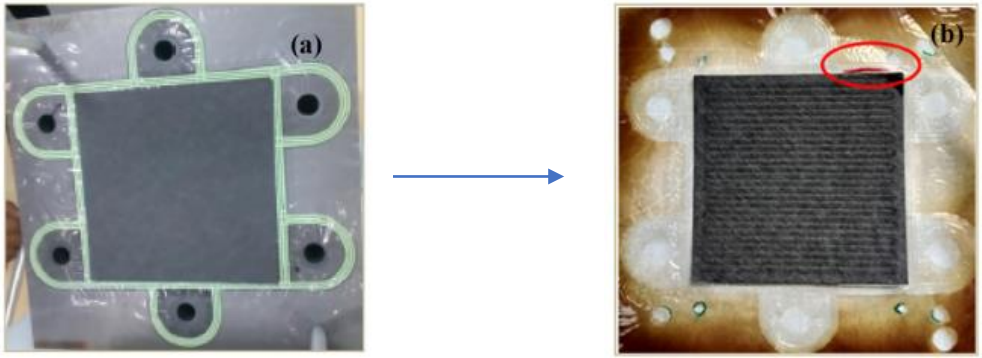

Meenakshi S. et al., International Journal of Hydrogen Energy, 48, 25, (2023), 9426-9435

Transmission geometry

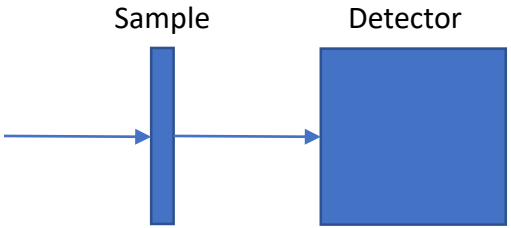

EXPERIMENTAL POSSIBILITIES

In situ analysis

Analysis are carried out in an environment which resamples and simulates the real environment of the electrode

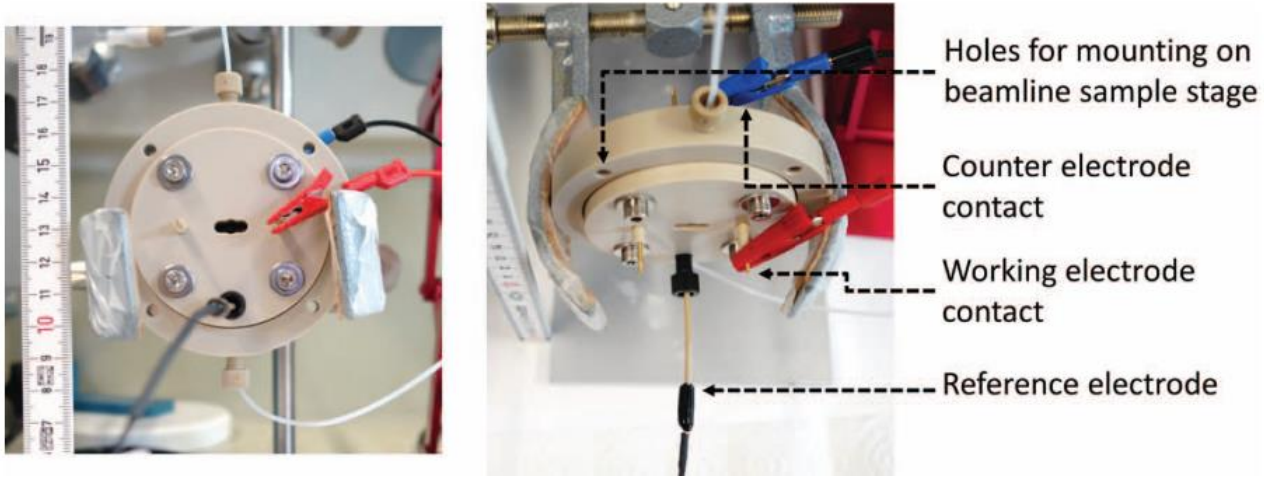

Binninger T. et al., Journal of The Electrochemical Society, 163, 10, (2016), H906-H912

EXPERIMENTAL POSSIBILITIES

In operando analysis

Analysis are carried out on a complete device in operative conditions

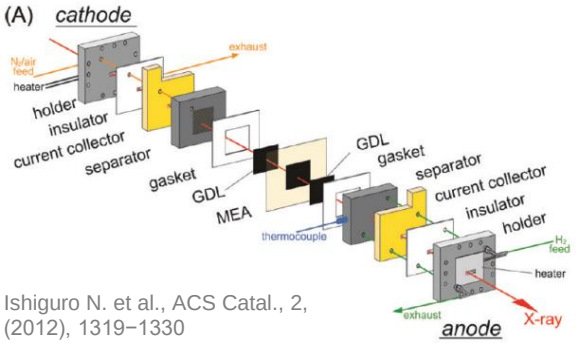

Ishiguro N. et al., ACS Catal., 2, (2012), 1319−1330

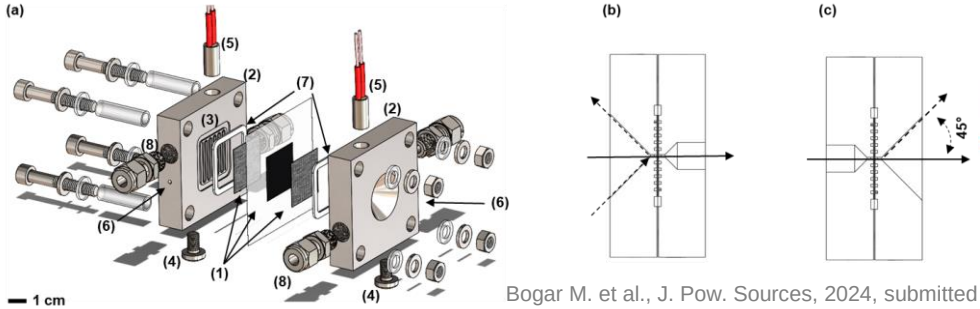

Bogar M. et al., J. Pow. Sources, 2024, submitted

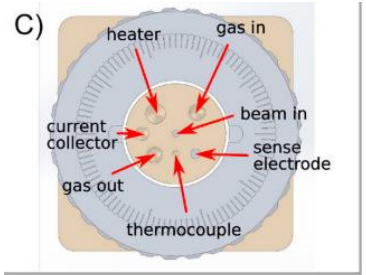

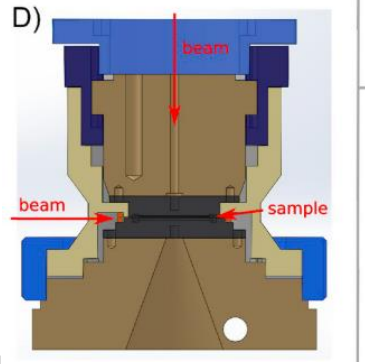

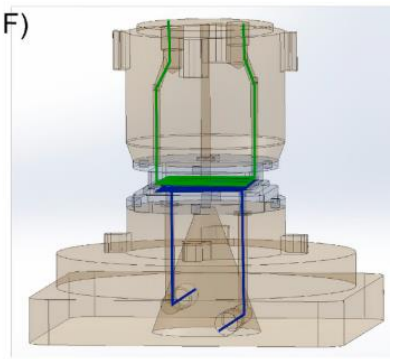

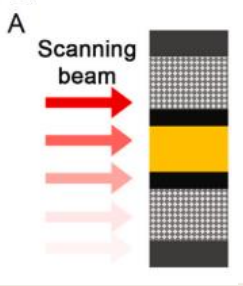

Martens I. et al. Journal of Power Sources 437 (2019) 226906

Martens I. et al., Journal of Power Sources 521, (2022), 230851

4. X-RAY ABSORPTION SPECTROSCOPY

X-RAY ABSORPTION SPECTROSCOPY

(a) Photoelectric absorption

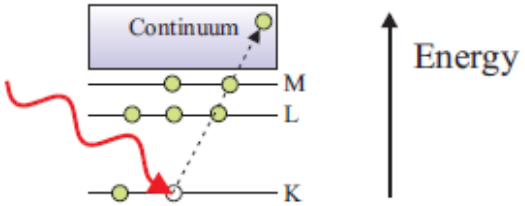

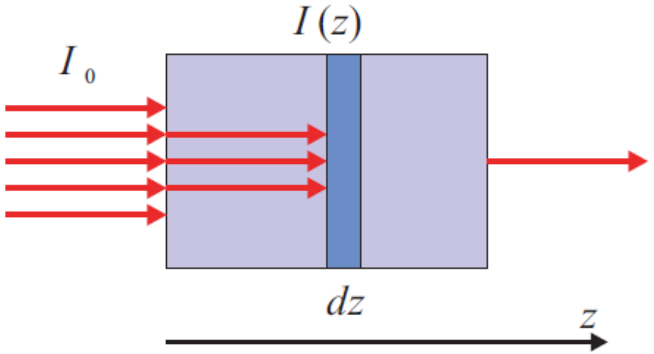

$$-dI = I(z)\,\mu\,dz$$

$$\frac{dI}{I(z)} = -\,\mu\,dz$$

$$I(z) = I_0 e^{-\mu z}$$

Nielsen, McMorrow, Elements of Modern X-ray Physics, Wiley (2011)

X-RAY ABSORPTION SPECTROSCOPY

$$\mu = \rho_{at}\,\sigma_{at} = \left(\frac{\rho_m\,N_A}{M}\right)\,\sigma_a$$

For composite materials

$$\mu = \sum_j \rho_{at,j}\,\sigma_{at,j}$$

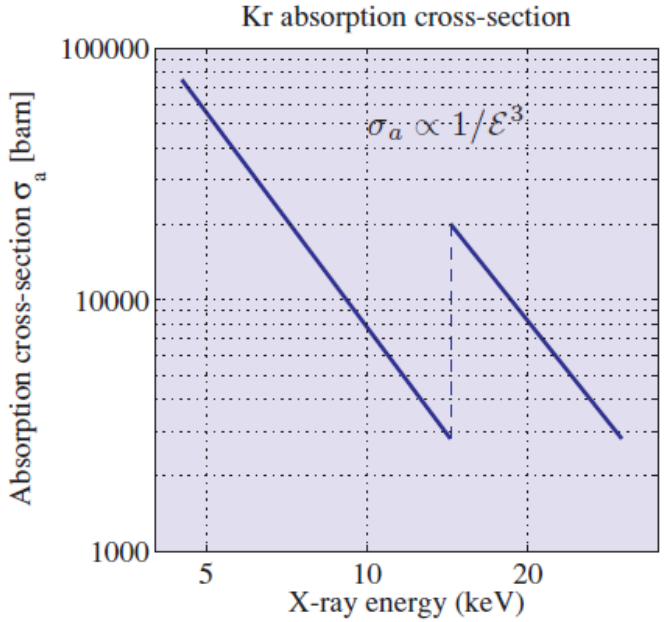

Nielsen, McMorrow, Elements of Modern X-ray Physics, Wiley (2011)

X-RAY ABSORPTION SPECTROSCOPY

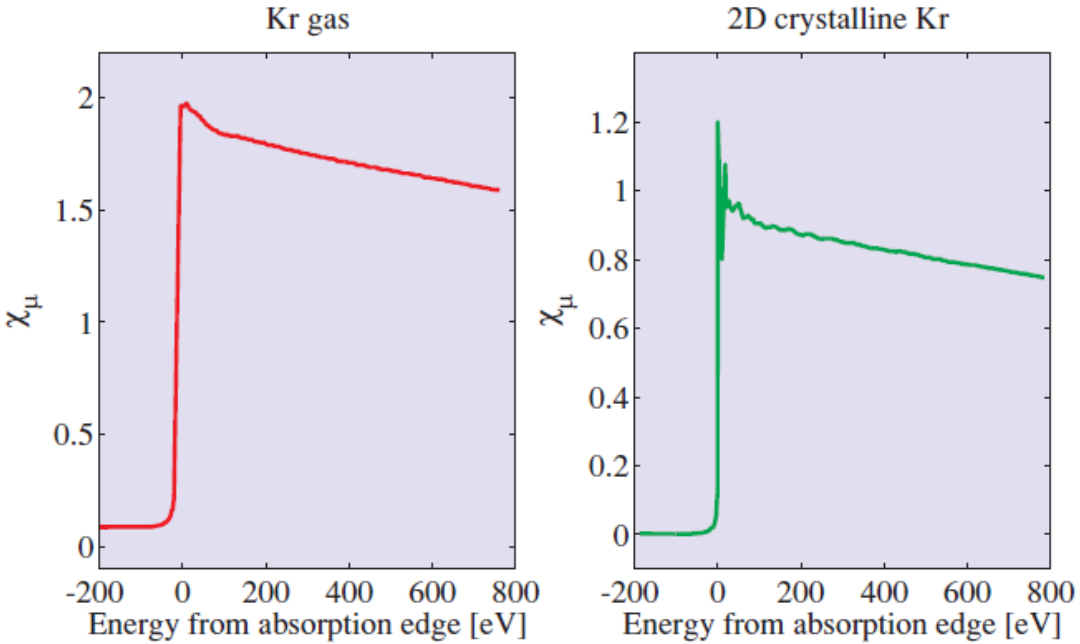

Nielsen, McMorrow, Elements of Modern X-ray Physics, Wiley (2011)

X-RAY ABSORPTION SPECTROSCOPY

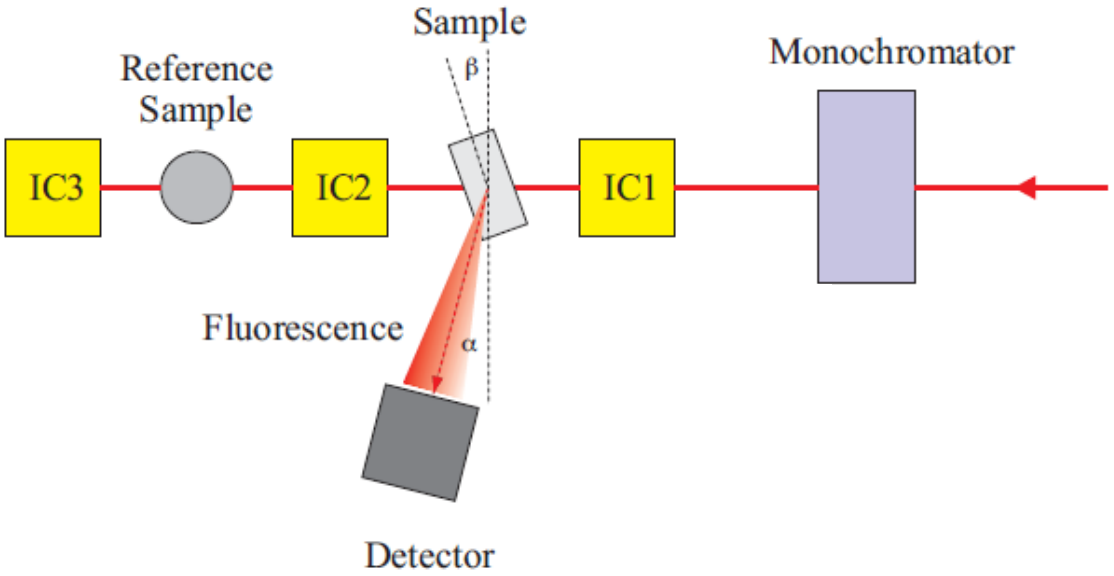

Nielsen, McMorrow, Elements of Modern X-ray Physics, Wiley (2011)

X-RAY ABSORPTION SPECTROSCOPY

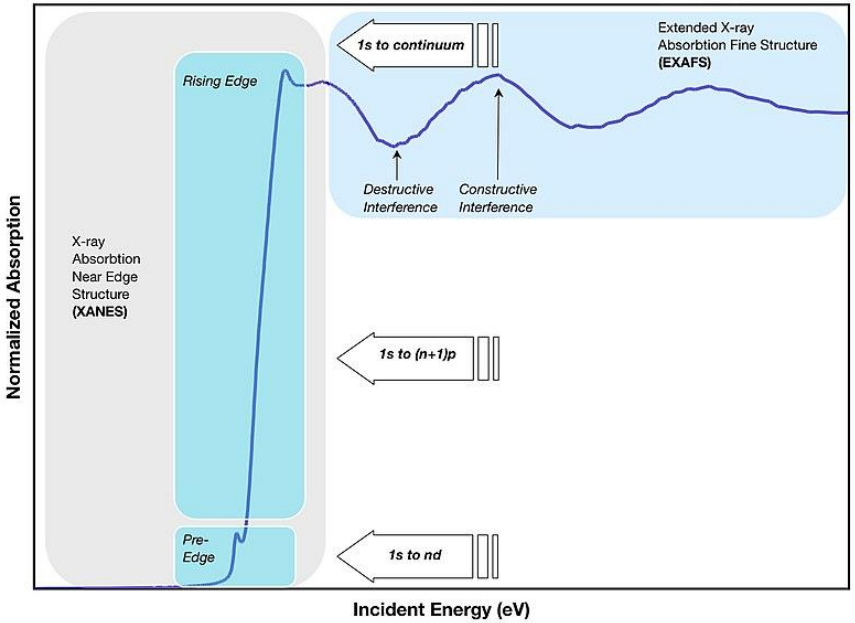

https://en.wikipedia.org/wiki/X-ray_absorption_spectroscopy

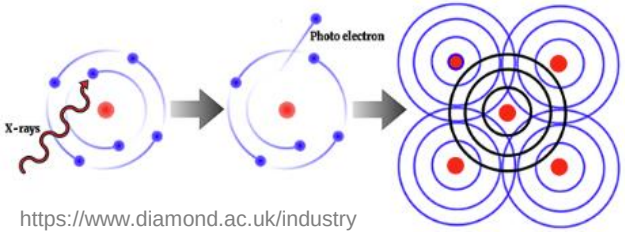

https://www.diamond.ac.uk/industry/Techniques-Available/Spectroscopy/X-ray-spectroscopy-XAS/About-XAS.html

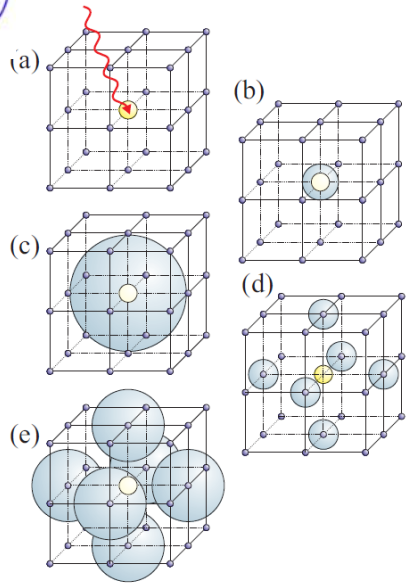

Nielsen, McMorrow, Elements of Modern X-ray Physics, Wiley (2011)

X-RAY ABSORPTION SPECTROSCOPY

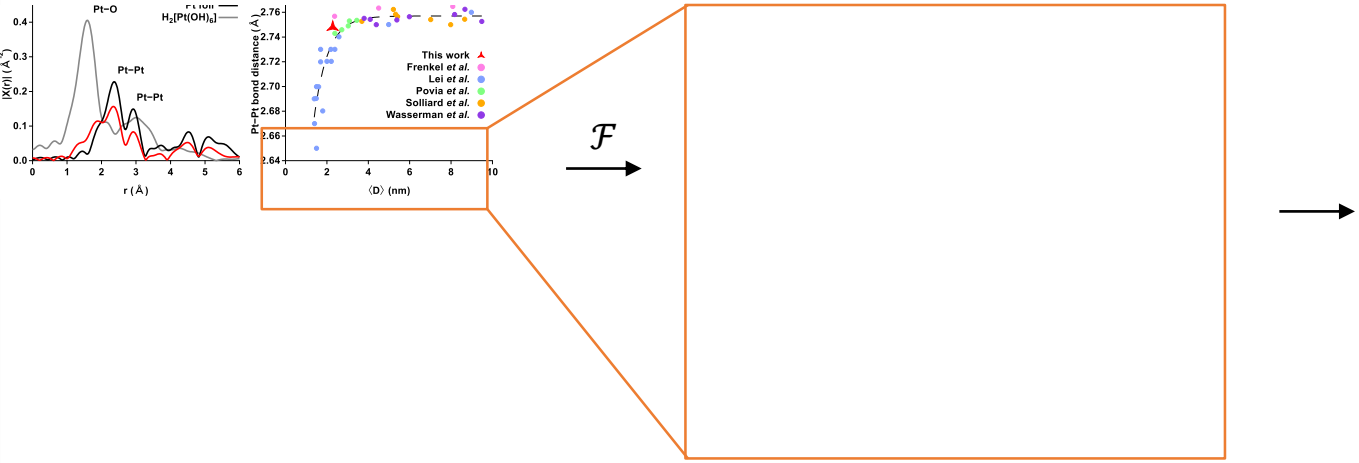

Bogar M. et al., J. Pow. Sources, 2024, submitted

X-RAY ABSORPTION / CASE OF STUDY

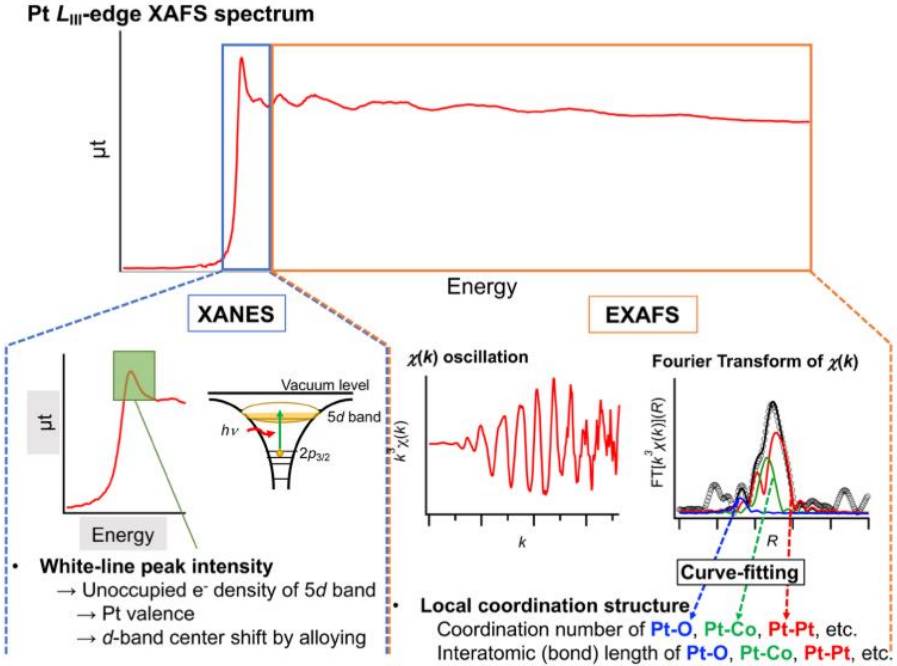

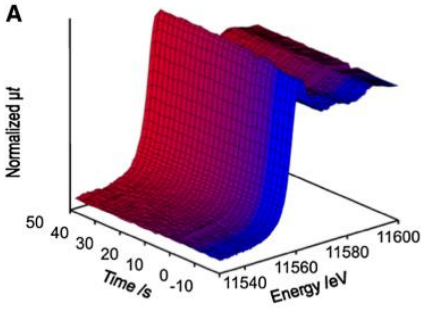

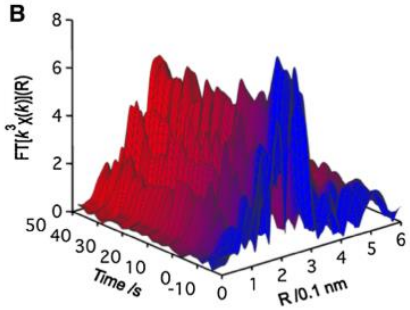

Ishiguro N. et al., J. Phys. Chem. C 2014, 118, 15874−15883

X-RAY ABSORPTION SPECTROSCOPY

Current (A)

White line height

$CN_{Pt\text{-}Pt}$

$CN_{Pt\text{-}M}$

$R_{Pt\text{-}Pt}$ (nm)

$CN_{Pt\text{-}O}$

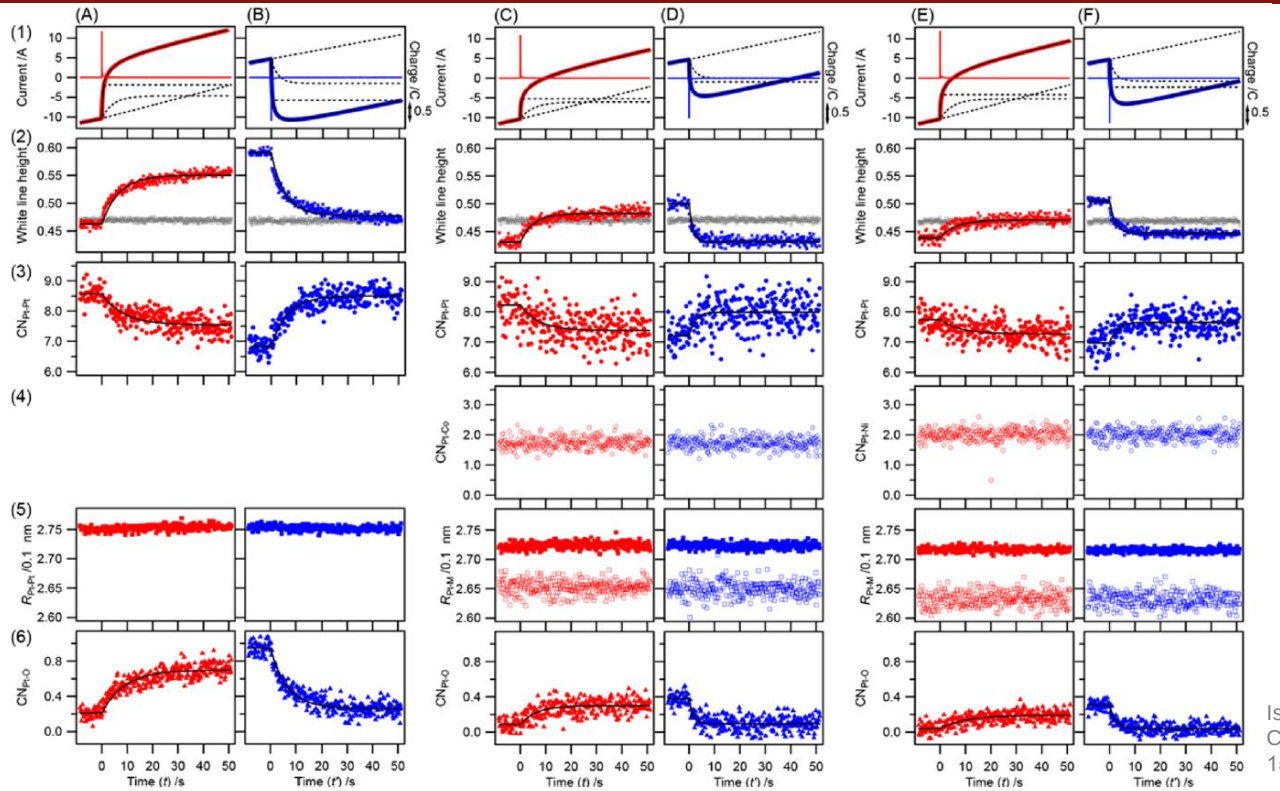

Ishiguro N. et al., J. Phys. Chem. C 2014, 118, 15874−15883

X-RAY ABSORPTION SPECTROSCOPY

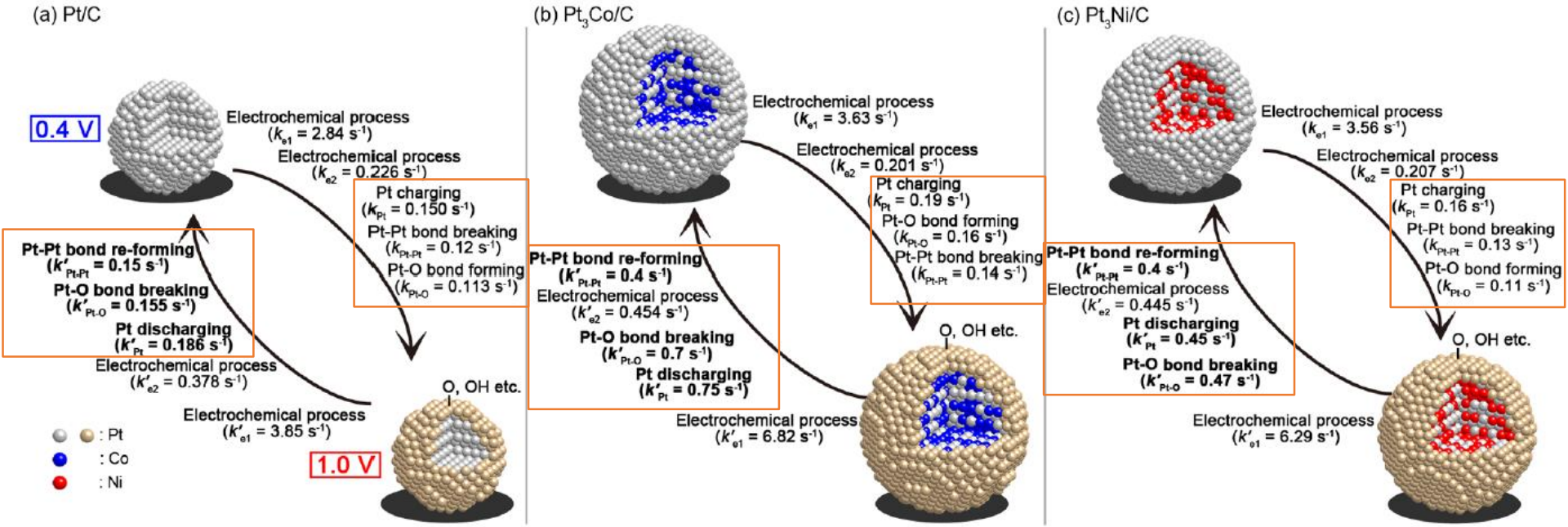

Ishiguro N. et al., J. Phys. Chem. C 2014, 118, 15874−15883

X-RAY DIFFRACTION AND SMALL ANGLE X-RAY SCATTERING

X-RAY DIFFRACTION

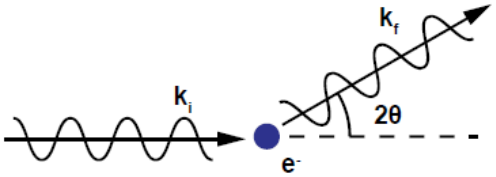

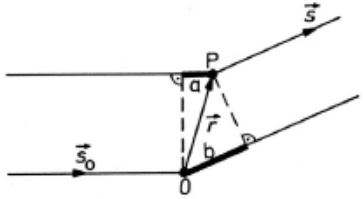

$a = \vec{r} \cdot \vec{s}_0$

$b = \vec{r} \cdot \vec{s}$

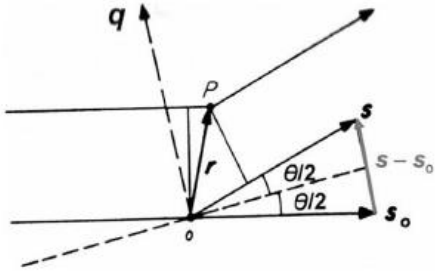

$$a - b = \boldsymbol{r s_0} - \boldsymbol{r s} = \boldsymbol{r}(\boldsymbol{s_0} - \boldsymbol{s})$$

$$\boldsymbol{q} = -\frac{2\pi}{\lambda}(\boldsymbol{s_0} - \boldsymbol{s}) \quad \rightarrow \quad \boldsymbol{q} = \boldsymbol{k} - \boldsymbol{k_0}$$

$$\varphi = -\frac{2\pi}{\lambda}\boldsymbol{r}(\boldsymbol{s_0} - \boldsymbol{s}) = -\boldsymbol{q r}$$

$$q = \frac{4\pi}{\lambda}\sin\frac{\theta}{2}$$

X-RAY DIFFRACTION

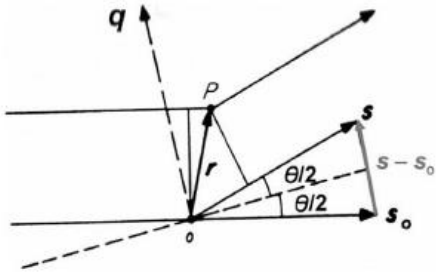

$$\boldsymbol{q} = -\frac{2\pi}{\lambda}(\boldsymbol{s_0} - \boldsymbol{s}) \quad \rightarrow \quad \boldsymbol{q} = \boldsymbol{k} - \boldsymbol{k_0}$$

$$\varphi = -\boldsymbol{q}\boldsymbol{r}$$

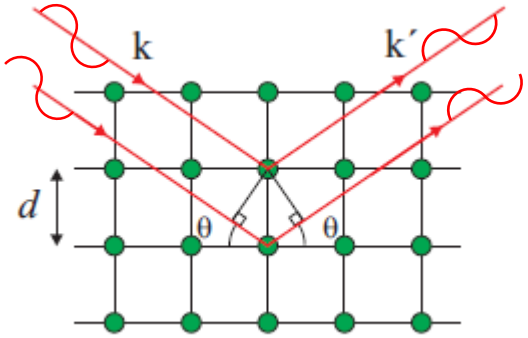

$$d = \frac{\lambda}{2}\sin\theta$$

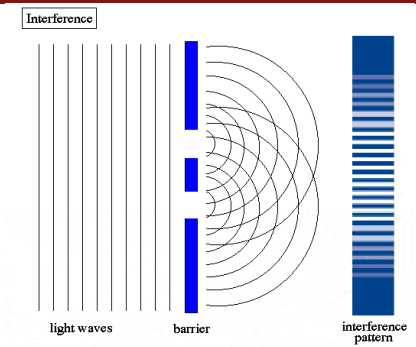

https://www.physicsforums.com/insights/what-is-the-double-slit-a-5-minute-introduction/

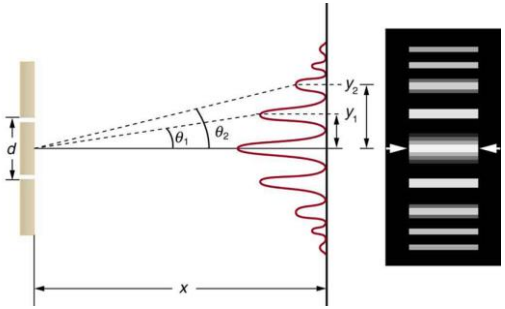

https://courses.lumenlearning.com/suny-physics/chapter/27-3-youngs-double-slit-experiment/

X-RAY DIFFRACTION

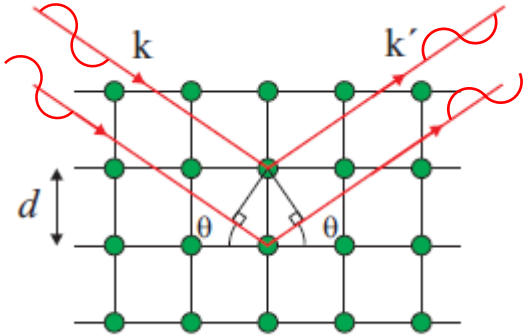

$$d = \frac{\lambda}{2}\sin\theta$$

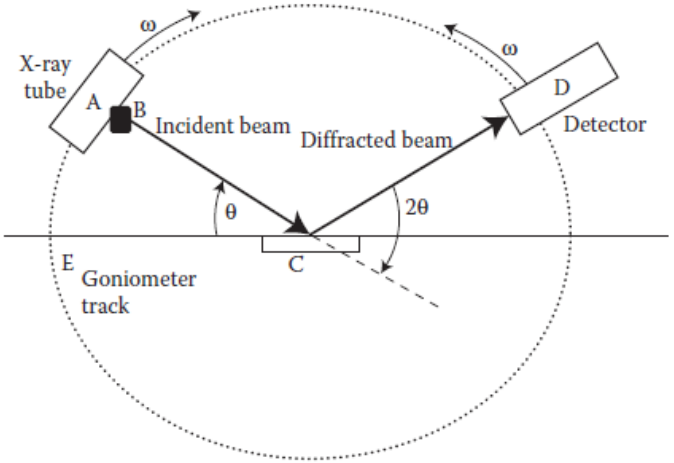

X-RAY DIFFRACTION

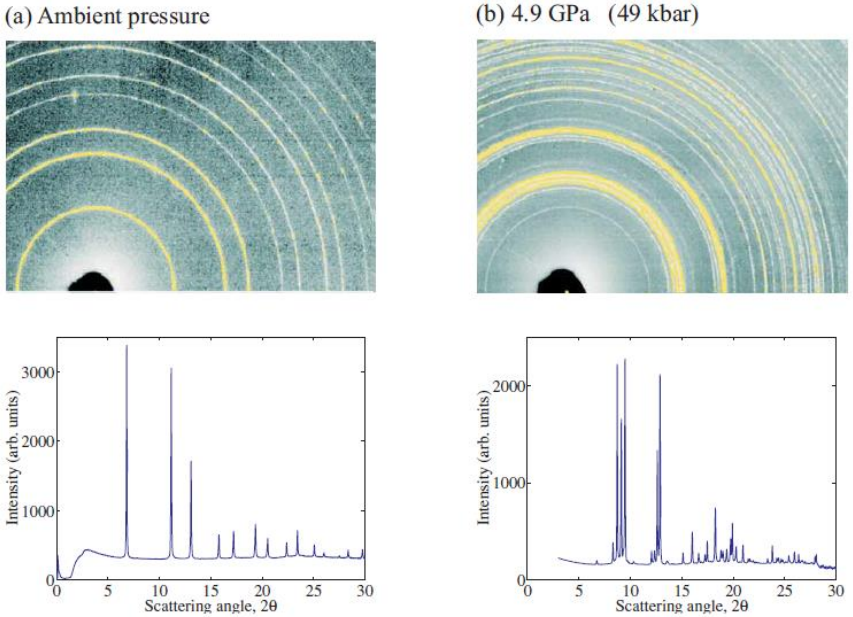

Fig. 5.24 Powder diffraction patterns from InSb at (a) ambient pressure, and (b) at a pressure of 4.9 GPa. The patterns recorded on an image plate detector are shown in the top row, and display rings where the detector intercepts the Debye-Scherrer cones. The data were recorded with an incident wavelength of $\lambda = 0.447$ Å. In the bottom row the radially averaged patterns as a function of 2θ are displayed. The results show that InSb undergoes a phase transition from the zinc sulfide structure to a phase with an orthorhombic structure at pressures above 4.9 GPa. (Data courtesy of Malcolm McMahon, University of Edinburgh.)

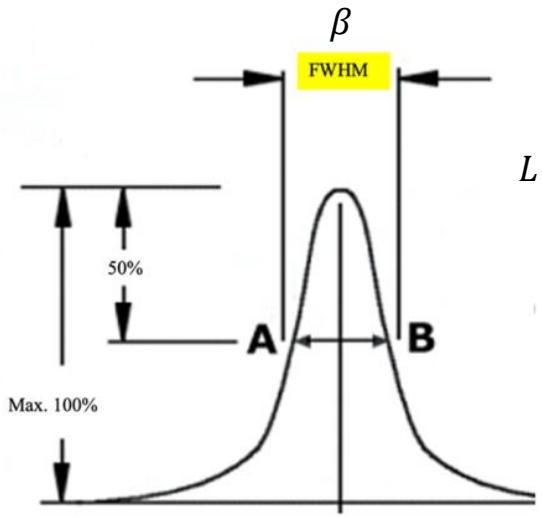

Debye-Sherrer formula

$$L = \frac{K\lambda}{\beta \cos\theta}$$

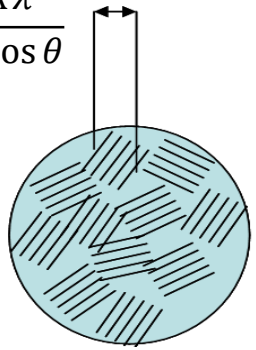

X-RAY DIFFRACTION AND SMALL ANGLE SCATTERING

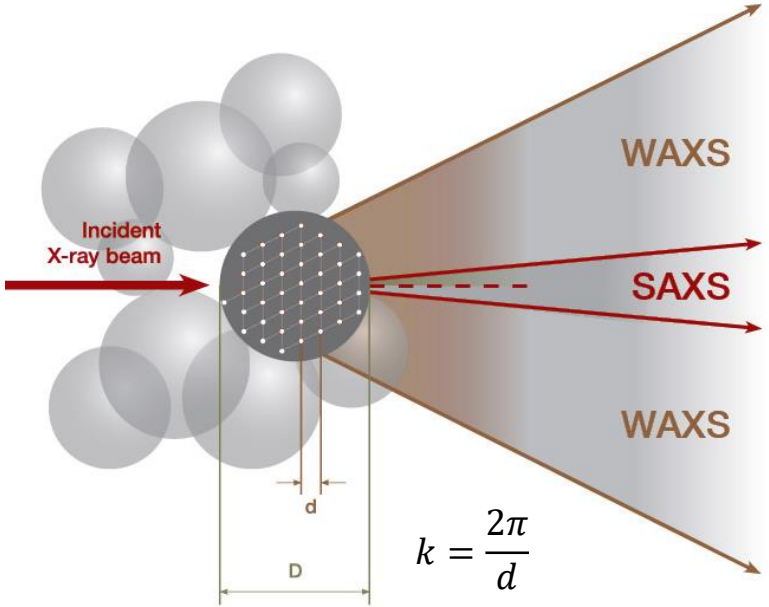

https://wiki.anton-paar.com/cn-cn/saxs-nanostructure-analysis/

SAXS

XRD

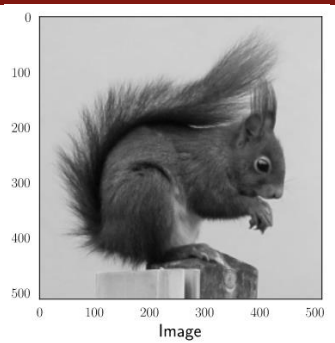

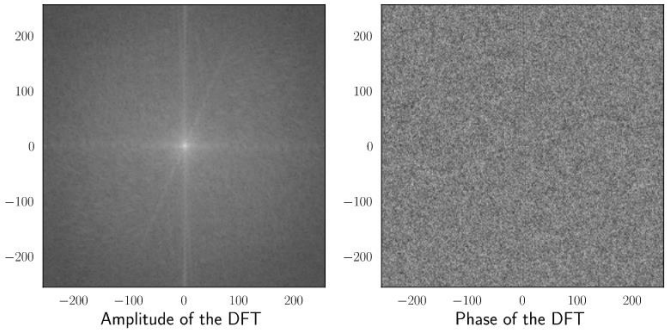

https://vincmazet.github.io/bip/filtering/fourier.html

Real space

Reciprocal space

X-RAY DIFFRACTION AND SMALL ANGLE SCATTERING

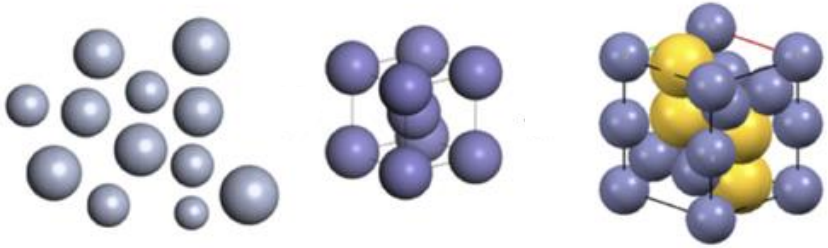

$$\rho(\boldsymbol{r})d\boldsymbol{r}$$

$$I(\boldsymbol{q}) = \int_V \rho(\boldsymbol{r})e^{-i\boldsymbol{q}\boldsymbol{r}}d\boldsymbol{r} = \mathcal{F}\{\rho(\boldsymbol{r})\}$$

Due to the similarity theorem of the Fourier transformation, we can call the space containing all position vectors **r** the real space, and the space containing the vectors **q** the reciprocal space.

SMALL ANGLE X-RAY SCATTERING

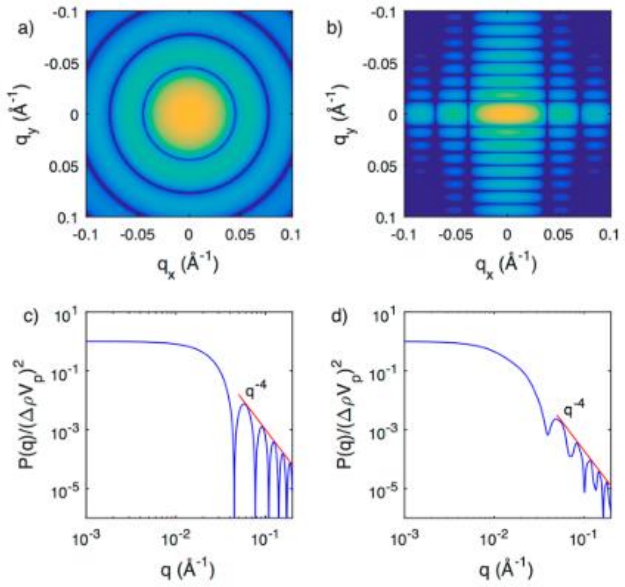

Figure 4. Two-dimensional (2D) scattering images (intensities are in log scale) of (a) sphere and (b) cylinder, where the axis of the cylinder is parallel to the *y*-axis. The 1D SAXS curves in (c) and (d) are the scatterings from randomly oriented spheres and cylinders, respectively. Intensities are normalized so that $P(0) = 1$. The radius of the sphere is 10 nm, and the radius and length of the cylinder are 10 and 50 nm, respectively.

Li T. et al., Chem. Rev. 2016, 116, 18, 11128–11180

$$I(\boldsymbol{q}) = P(\boldsymbol{q})S(\boldsymbol{q})$$

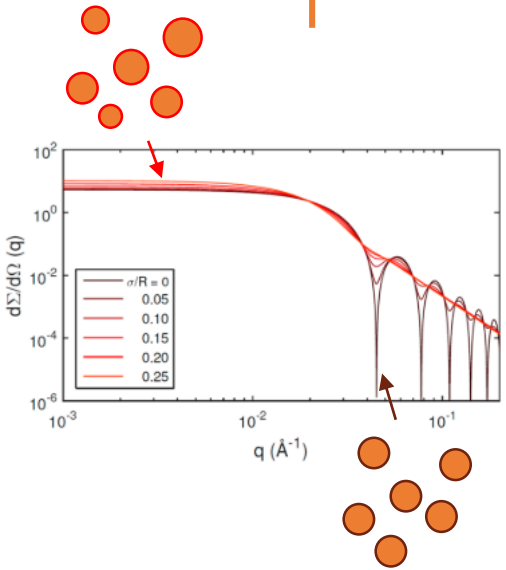

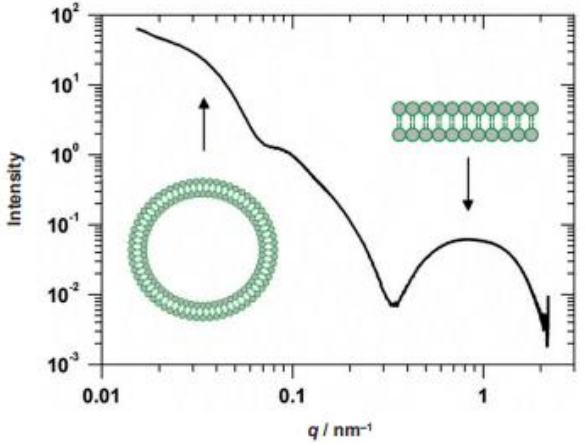

Richter M., Ulm G., PTB-Mitteilungen 124 (2014), No. 3 / 4

SMALL ANGLE X-RAY SCATTERING

$$I(\boldsymbol{q}) = P(\boldsymbol{q})S(\boldsymbol{q})$$

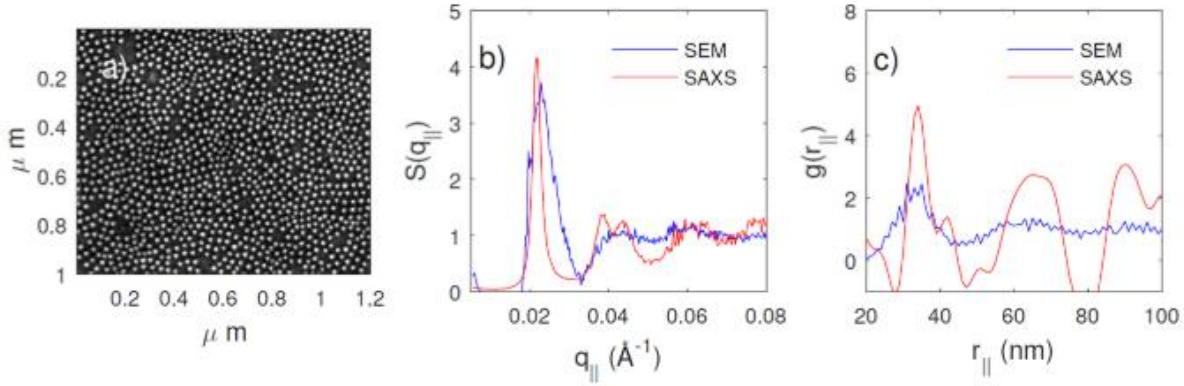

Figure 14. (a) SEM image of 15 nm DNA-conjugated gold nanoparticles (DNA–AuNPs) hybridized to DNA modified substrates. (b) Structure factors calculated from SEM and experimental SAXS data. (c) The pair distribution function calculated from the structure factor in (b) shows sharper peaks and clearer hexagonal symmetry than the pair distribution function calculated from the SEM in (a), likely because of better statistics. Reproduced from ref 129. Copyright 2014 American Chemical Society.

Li T. et al., Chem. Rev. 2016, 116, 18, 11128–11180

SMALL ANGLE X-RAY SCATTERING

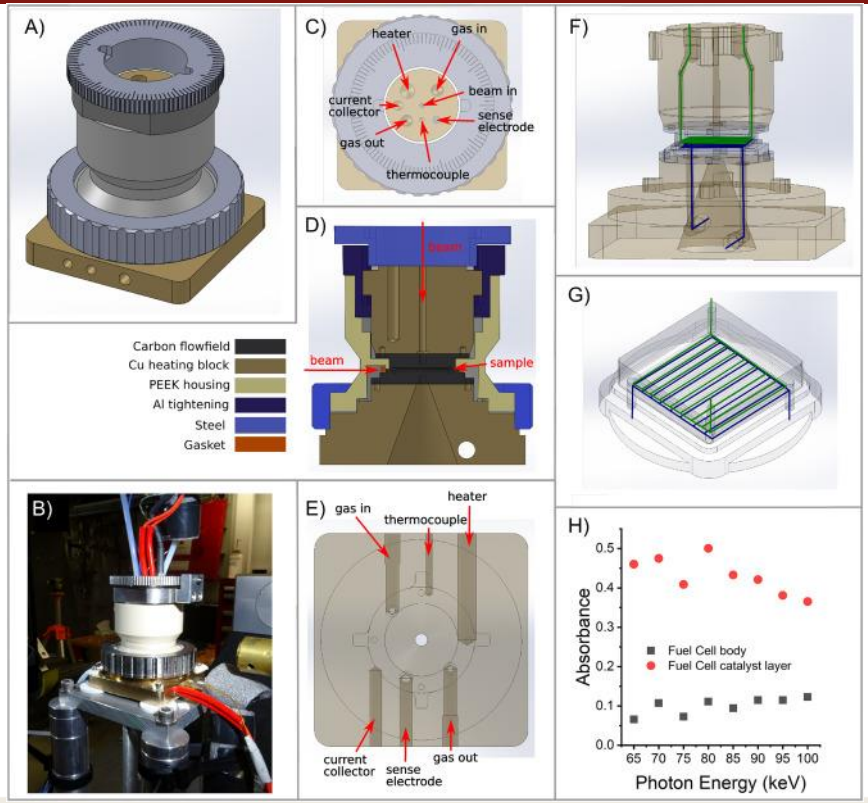

Martens I. et al., Journal of Power Sources 521 (2022) 230851

SMALL ANGLE X-RAY SCATTERING

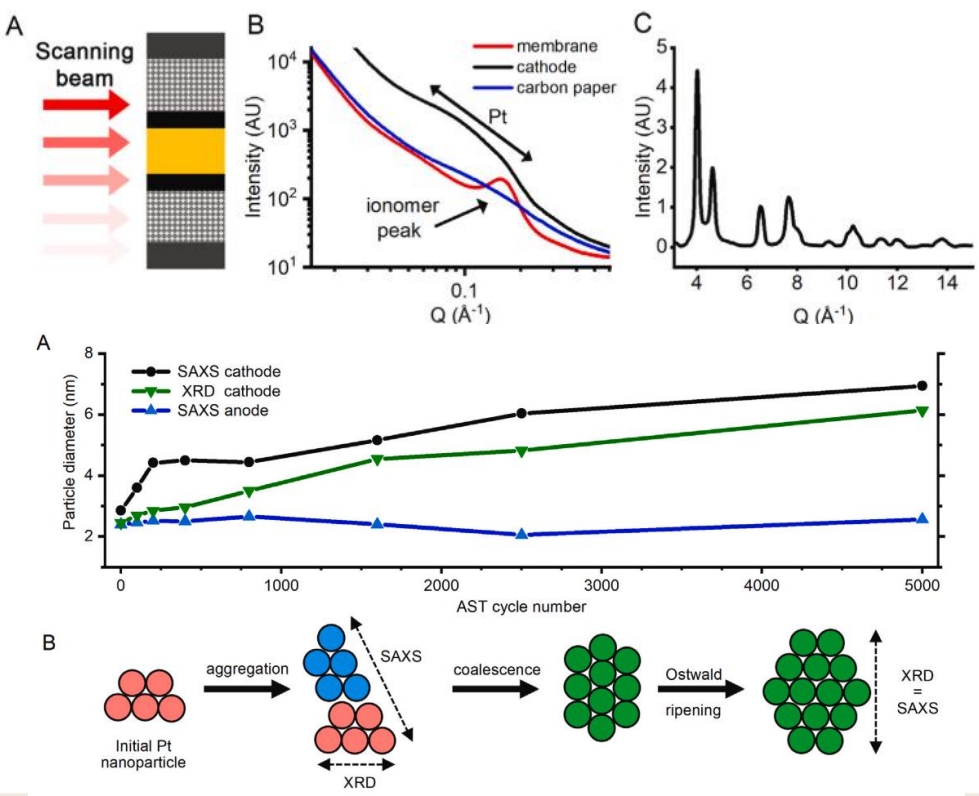

Martens I. et al., Journal of Power Sources 521 (2022) 230851

SMALL ANGLE X-RAY SCATTERING IN GRAZING INCIDENCE CONDITIONS

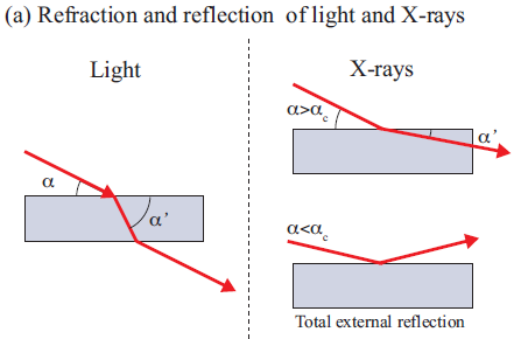

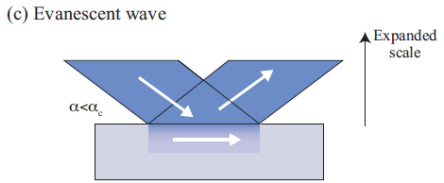

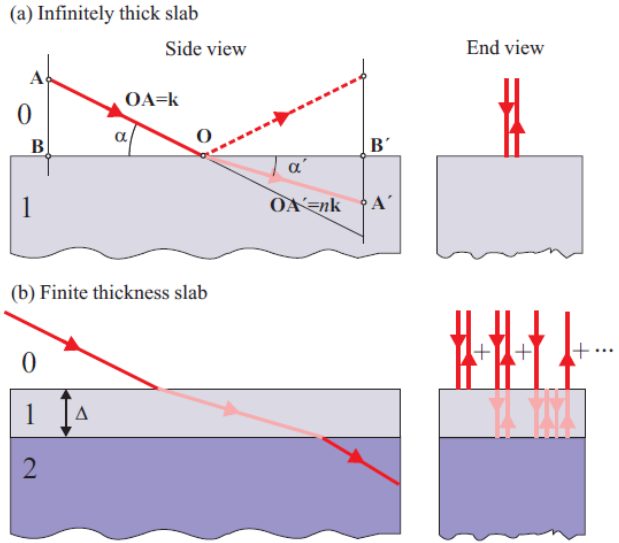

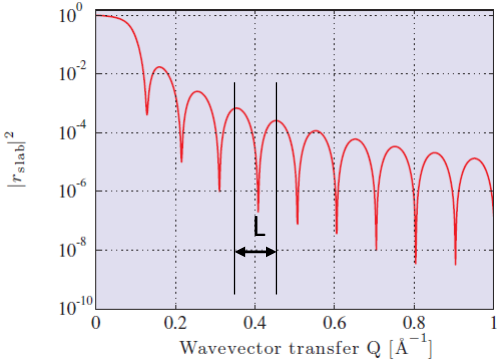

$$\Delta = \frac{2\pi}{L}$$

Nielsen, McMorrow, Elements of Modern X-ray Physics, Wiley (2011)

SMALL ANGLE X-RAY SCATTERING

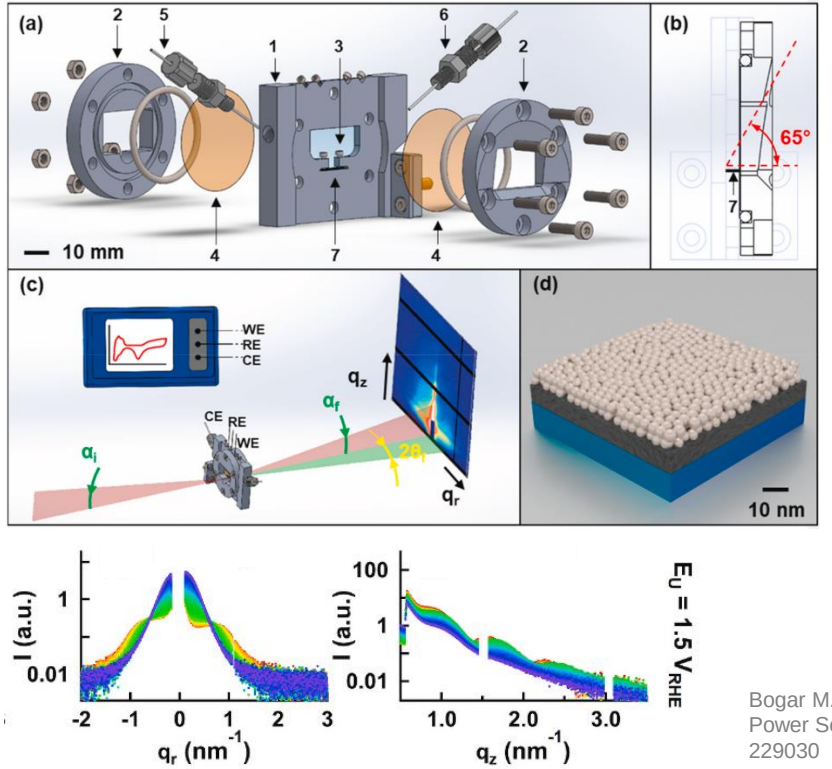

Bogar M. et al., Journal of Power Sources 477 (2020) 229030

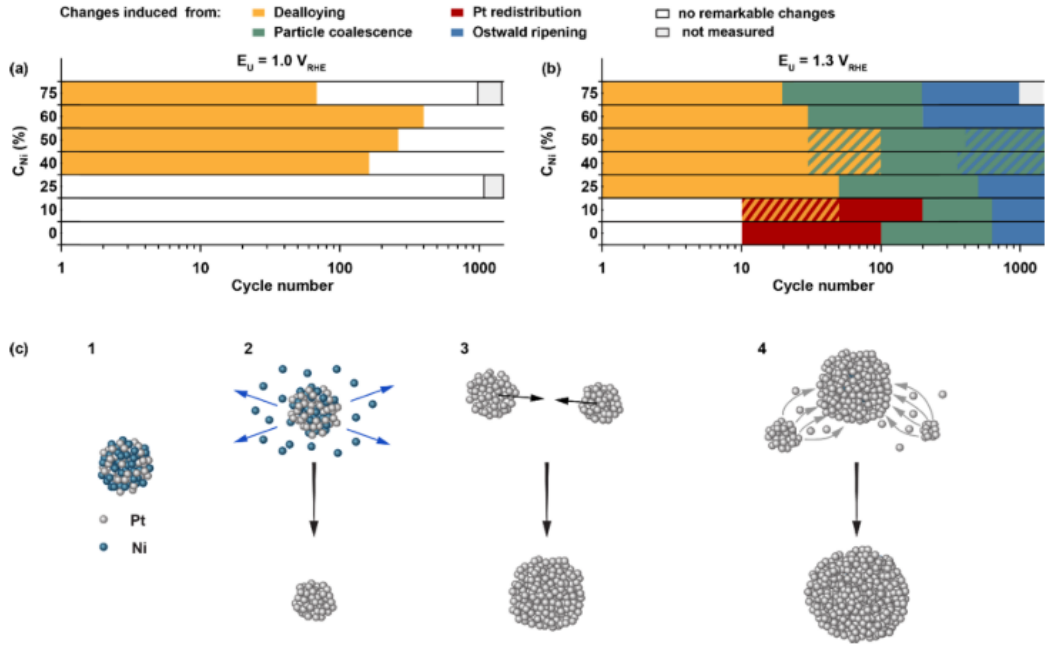

Bogar M. et al., ACS Catal. 2021, 11, 11360−11370

5. NEUTRON BASED CHARACTERIZATION TECHNIQUES

NEUTRON SCATTERING

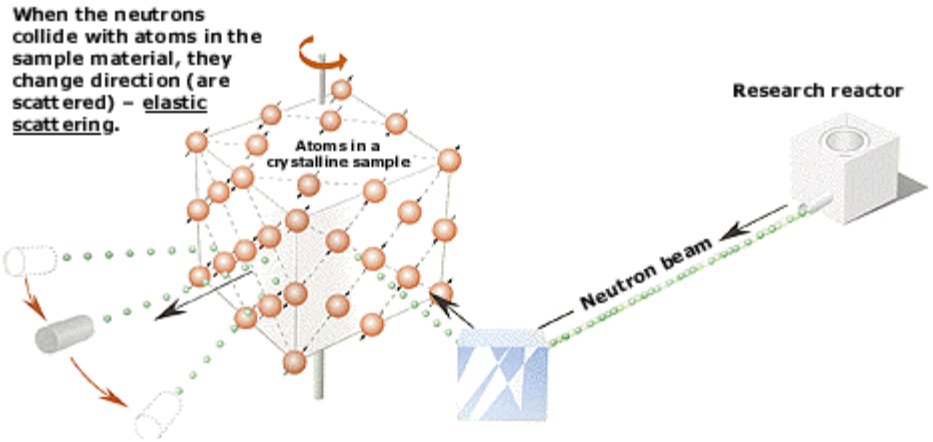

https://www.psi.ch/en/sinq/hrpt/neutron-diffraction-practicum

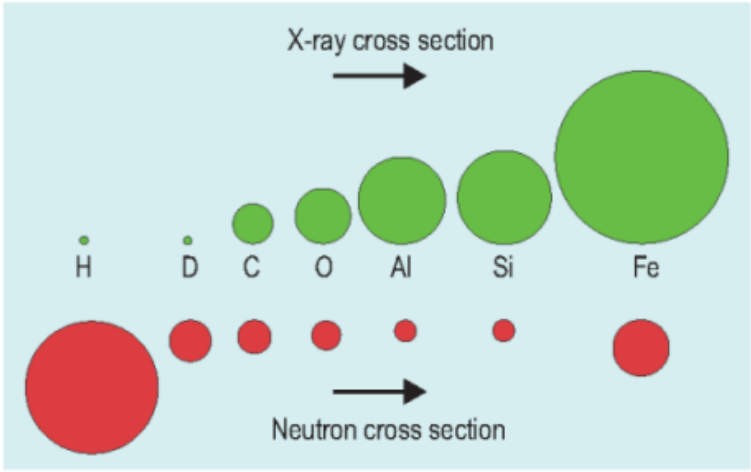

Fig. 2. Neutron and x-ray scattering cross-sections compared. Note that neutrons penetrate through Al much better than x rays do, yet are strongly scattered by hydrogen.

https://www.ncnr.nist.gov/AnnualReport/FY2003_html/RH2/

NEUTRON SCATTERING

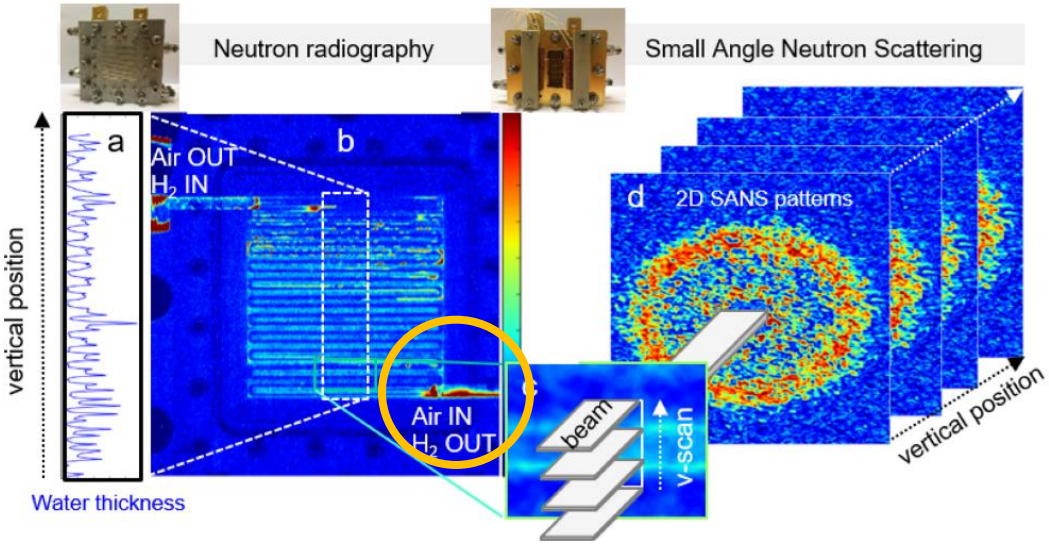

Martinez N. et al., ACS Appl. Energy Mater. 2019, 2, 8425−8433 Article

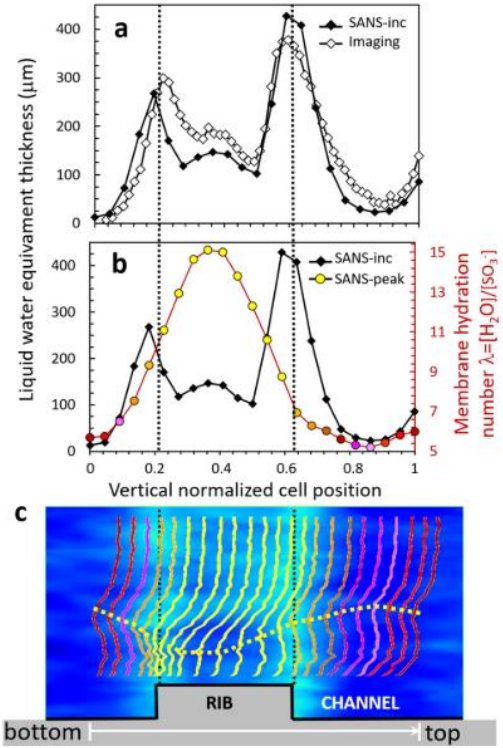

THESIS RELATED TO FUEL CELLS AND WATER ELECTROLYSERS

UNIVERSITÀ
DEGLI STUDI
DI TRIESTE

Dipartimento di
Ingegneria
e Architettura